2nd Workshop Of
CODE_BRIGHT USERS

6th – 7th May 2010
Barcelona, Spain

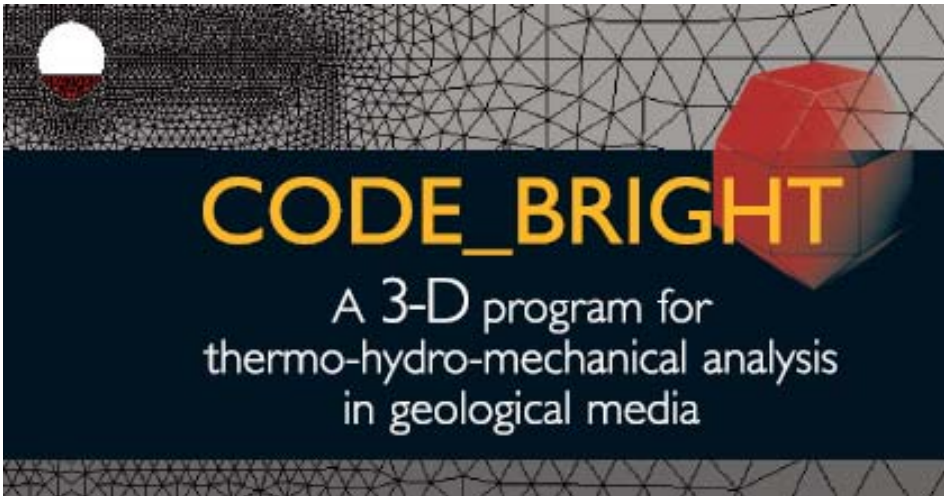

Department of Geotechnical Engineering and Geosciences
(UPC. Barcelona. Spain)
CIMNE
(Centro Internacional de Métodos Numéricos en Ingeniería.
Barcelona. Spain)

CODE_BRIGHT

A 3-D program for thermo-hydro-mechanical analysis in geological media

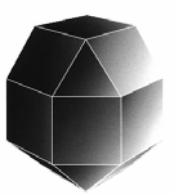

2ND WORKSHOP OF CODE_BRIGHT USERS

Barcelona, 6-7 May 2010

Department of Geotechnical Engineering and Geosciences
(UPC. Barcelona. Spain)

CIMNE
(Centro Internacional de Métodos Numéricos en Ingeniería. Barcelona. Spain)

CONTENTS

PREDICTION OF LONG-TERM COMPACTION OF SALT BACKFILL IN HLW DISPOSAL BOREHOLES IN ROCK SALT

Mingliang XIE* and Chun-Liang ZHANG*

* Gesellschaft für Anlagen- und Reaktorsicherheit (GRS), D-38122 Braunschweig, Germany
e-mail: xie@grs.de, web page: http://www.grs.de/

Key words: Thermo-mechanical coupled process, rock salt, crushed salt

Abstract. *This paper provides the numerical prediction of the long-term consolidation process of crushed salt as backfill in a deep repository of high-level radioactive waste (HLW) in rock salt. The related porosity and permeability changes of the backfill are calculated by considering the coupled thermo-mechanical processes in the rock – buffer barrier system surrounding HLW disposal boreholes. The modeling results suggest that a very low porosity of 1% will be reached over 1000 years and the corresponding permeability will decrease to about* 10^{-18} m^2.

1 INTRODUCTION

Rock salt is a potential host rock for HLW repositories in Germany owing to its favorite properties like negligible permeability, visco-plasticity, and high self-sealing potential of the excavation-induced damage. In the disposal concept [1], HLW canisters will be emplaced in vertical boreholes of 300 m in depth and 0.6 m in diameter, which will be located in depths of 800 m to 1100 m below the ground surface. The boreholes will be backfilled with crushed salt produced by the excavation. A consolidation process can be expected in the backfill due to the creep deformation of the rock salt under the high lithostatic stresses of 18 to 25 MPa. The compaction process will be accelerated by high temperatures up to 200°C generated by the heat transfer from the waste. The consolidation process of the backfill has been predicted by coupled thermo-mechanical modeling under consideration of the rock - buffer barrier system surrounding a HLW disposal borehole. CODE-BRIGHT is used in the modeling.

2 CONTITUTIVE LAWS

The constitutive models for the mechanical behaviour of saline materials implemented in CODE-BRIGHT [2] are adopted for both rock salt and crushed salt. Assuming the normal repository conditions without brine intrusion, elastic deformation, and dislocation creep of the rock and creep compaction of the backfill are taken into account under dry conditions. The backfill can theoretically be compacted so far to the intact rock, i.e. the porosity tends to zero. The thermal conductivity in Fourier's law for the computation of conductive heat flux is dependent on porosity and temperature. Details of the models are described in literature [2].

3 MATERIAL PROPERTIES

- Thermal parameters for rock salt and crushed salt are the same, but denpeding on porosity ϕ and temperature T: $\lambda_{dry} = \lambda_{solid}^{(1-\phi)} \lambda_{gas}^{\phi}$, $\lambda_{solid} = (\lambda_{solid})_o + a_1 T + a_2 T^2 + a_3 T^3$

$\lambda_{solid} = 5.73$ *W.m/K,* $\lambda_{gas} = 0.1$ *W.m/K,* $a_1 = -1.838 \cdot 10^{-2}$, $a_2 = 2.86 \cdot 10^{-5}$ and $a_3 = -1.51 \cdot 10^{-8}$.

- The elastic modulus is related with the porosity change: $E = E_o + (\phi - \phi_o)\frac{dE}{d\phi} \geq E_{\min}$

Description	Unit	Crushed Salt	Rock Salt	Canister
Young Modulus E0	MPa	200	25000	250000
Variation of E, dE/dϕ	J mol^{-1}	-5000	0	0
Poission's ratio ν	-	0.27	0.27	0.27

- The dislocation creep model and parameters are:

$$\frac{d\varepsilon^{DC}}{dt} = \frac{1}{\eta_{DC}^{d}}\Phi(F)\frac{\partial G}{\partial \sigma'}, \quad F = G = \sqrt{q^2 + \left(\frac{-p}{\alpha_p}\right)^2} \quad \Phi(F) = F^n \quad \alpha_p = \left(\frac{\eta_{DC}^{v}}{\eta_{DC}^{d}}\right)^{\frac{1}{n+1}}$$

$$\frac{1}{\eta_{DC}^{v}} = A(T)g_{DC}^{v}(e) \qquad \frac{1}{\eta_{DC}^{d}} = A(T)g_{DC}^{d}(e) \qquad g_{DC}^{v}(e) = 3(G-1)^n f$$

$$g_{DC}^{d}(e) = \left(\sqrt{\frac{1+g+g^2}{3}}\right)^{n-1}\left(\frac{2g+1}{3}\right)f + \frac{1}{\sqrt{g}} \qquad g = \frac{1}{(1-f)^2} \qquad f = \sqrt{\frac{2e}{3(1-e^{3/2})(1+e)}}$$

$$A(T) = A_A \exp\left(\frac{-Q_A}{RT}\right)$$

in which e is void ratio. The initial void ration (e_0) in the rock salt is assumed to be 0.01, and e_0 =0.43 in the backfill. $A_A = 2.08\cdot10^{-6}$ s^{-1}MPa^{-n}, Q_A=54000 J mol^{-1}, and n=5.

- The permeability (k) – porosity (ϕ) relationship [3]: $k=1.12\cdot10^{-8}\,\phi^{5.25}$.

4 NUMERICAL SIMULATION

4.1 Model set-up

The geometry and model set-up are schematically described in Figure 1. A 2D axisymmetric model was adopted for a large rock mass with 23.5 m in radius and 300 m in height. The gallery locates at 800 m beneath the ground surface [1], from which a borehole of 0.6 m in diameter is drilled vertically to a depth of 100 m. Totally 19 canisters of type BSK3 are laid on top of each other. The narrow vertical gap between canister and rock salt has a thickness of 0.085 m and filled with crushed salt. On top of the borehole, there is a salt block with a height in 10 m and the same diameter of canister (0.215 m) for covering and sealing purposes. The gallery is also filled with the crushed salt.

Based on this concept, the following initial and boundary TM conditions are set up for the numerical simulation.

1. Along the symmetric axis (r=0) and on the outer boundary at r = 23.5 m, no horizontal deformation is allowed (Figure 1, right), while no vertical deformation is prescribed on the bottom boundary (200 m below the gallery). At the top boundary (100 m above the gallery), an overburden stress of 13 MPa is applied.
2. The initial temperature was linearly distributed along the depth with 35°C on the top

and 40°C on the bottom boundary. The delayed heat power from the BSK3-type canister is applied along the outer surface of the canisters in the borehole. The time evolution of the heat from a BSK3-canister is depicted in Figure 2.

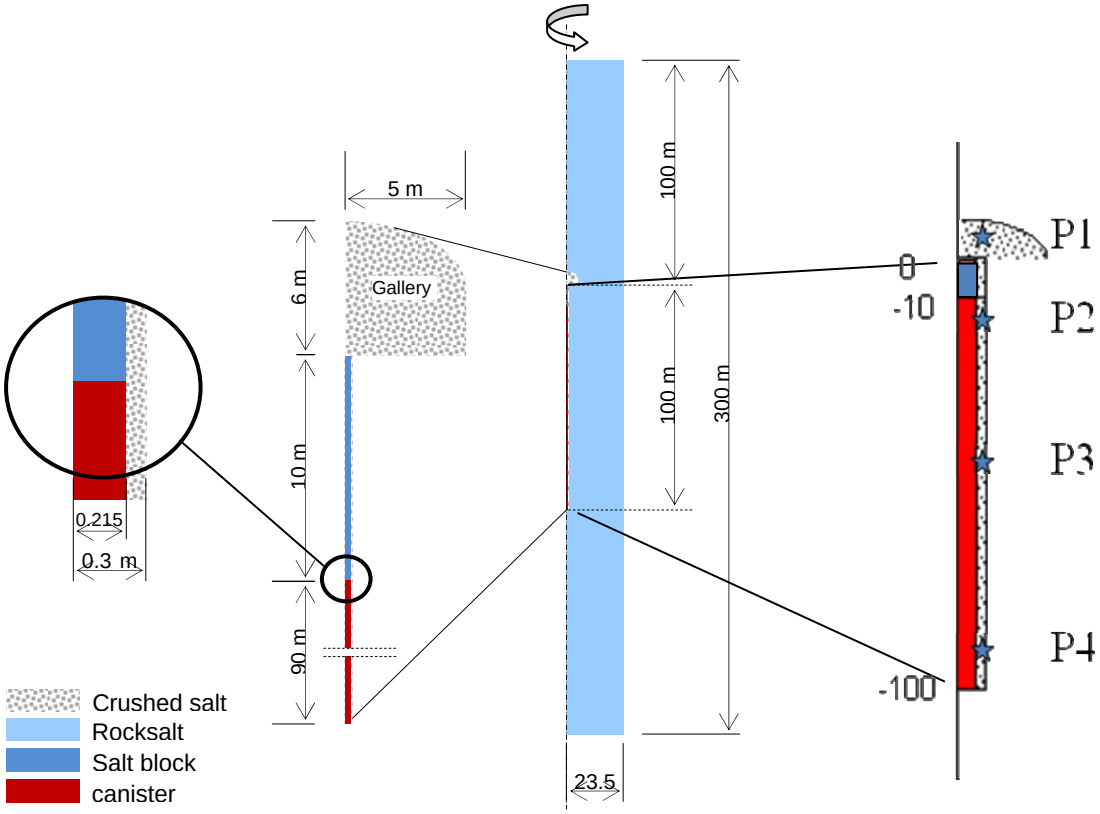

Figure 1: 2D axisymmetrical model and selected points in the gallery (P1) and in the backfill within the borehole (P2-P4)

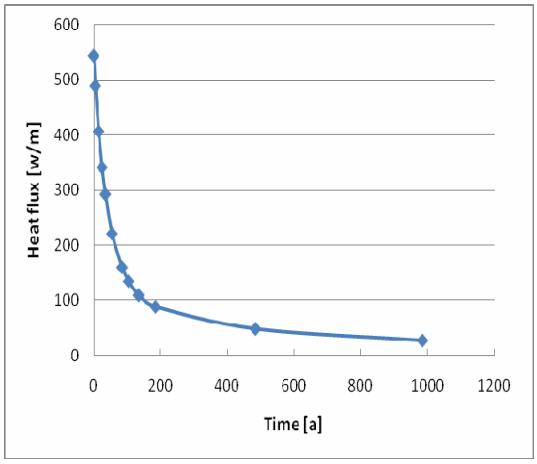

Figure 2: Heat flux of the canister after a storage period of 15 years

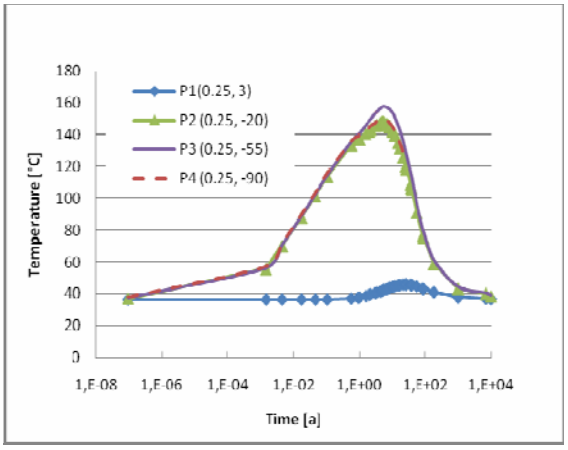

Figure 3: Temperaure evolution at selected points

4.2 Results

The temperature evolution calculated for several typical points are shown in Figure 3. The peak temperature at observation point P3 with coordination (r=0.25m, y=-55m) is reached

almost 160°C after about 6 years. This point is located in the backfill at the middle depth of the HLW borehole. The peak temperature reached in the backfilled gallery (point P1) is much lower with about 46°C.

The evolution of the backfill compaction at some selected points is illustrated in Figure 4 (left). The porosity decreases gradually with time. In the heated area around the HLW borehole, the compaction rate is much faster than in the gallery with lower temperature. After 100 years a very low porosity of about 1.5% is reached in the heated, while the remaining porosity in the backfill in the less heated area in the gallery is much higher area with 23%. Correspondingly, the calculated permeability for the backfill in the borehole reaches to 1E-18 m^2 over the first 100 years. Further reduction seems to be very low and takes over 1000 years to reach a porosity of 1% in heated area. It is to be noted that the permeability data were obtained by gas flowing. It may be different from that obtained by brine flowing. The effect of wetting by brine intrusion will be investigated in the future.

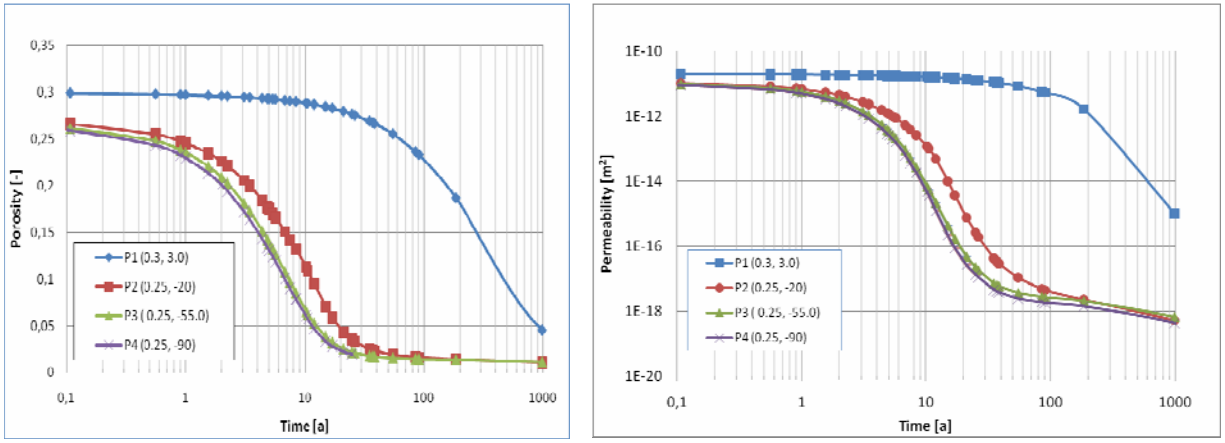

Figure 4: Predicted porosity (left) and gas permeability (right) evolution at observation points

6 CONCLUSION AND REMARKS

The numerical prediction indicates that the crushed salt backfill in HLW boreholes can be gradually consolidated by the creep of the host rock especially under elevated temperatures. The compaction reduces the porosity and permeability. Over 1000 years, the porosity reaches to a very low value of 1% and the related permeability decreases to about 10^{-18} m^2.

7 ACKNOWLEDGMENT

The authors gratefully acknowledge the funding of the REPOPERM project (02 E 10477) by the German Federal Ministry of Economics and Technology (BMWi).

REFERENCES

[1] Rothfuchs, T., Droste, J. et al (2004): A basis for evaluation and developing concepts for final repositories for high-level radioactive waste – CROP Cluster Repository Project – German country annexes. GRS-201.

[2] Olivella & Gens (2002): A constitutive model for crushed salt, Int. J. Numer. Anal. Meth. Geomech. 26:719-746.

[3] Zhang, C.-L., Rothfuchs, T. und Droste J.: Post-Tests on thermo-mechanically compacted salt backfill. In: Wallner et al.(eds.) The mechanical behaviour of salt: understanding of THMC processes. Proc. of the 6th conf. On the mechanical behaviour of "saltmech6", Hannover, Germany. Taylor & Francis Group, London, pp 209-214, 2007.

INTERPRETATIVE MODELING OF SELECTED IN SITU MEASUREMENTS OBTAINED AT URL MONT TERRI USING CODE_BRIGHT

O. Czaikowski, K. Wieczorek and R. Miehe

Gesellschaft für Anlagen und Reaktorsicherheit (GRS)
Theodor-Heuss-Strasse 4, 38122 Braunschweig, Germany
e-mail: oliver.czaikowski@grs.de, web page: http://www.grs.de

Key words: in situ measurements, HM coupled analysis, URL Mont Terri

Abstract. *Regarding the tight coupling between fluid flow processes and mechanical deformation in argillaceous rock mass this paper presents selected experimental findings obtained in the URL Mont Terri which are interpreted in terms of physical modeling and numerical simulation using CODE_BRIGHT. Within the interpretative modelling process, 2D and 3D numerical modelling work, reflecting the actual properties of the rock in situ, is performed and the simulation results are compared to the experimental findings.*

1 INTRODUCTION

The international experience gained in the field of geological radioactive waste disposal indicates that coupling between thermal, hydraulic, mechanical and chemical processes (THMC-coupling) in claystone rock mass will be much more significant than in salt rock formations. The fabric components, saturation level and pore water pressure determine the load bearing behavior of the claystone rock mass affected by the impact of excavation activity and waste storage related aspects.

It is widely agreed that the overall detection of geohydraulic conditions and their changes due to geomechanical disturbances via in situ measurements is one of the most relevant prerequisites for reliable physical modeling and numerical simulation of coupling processes. With respect to disposal in argillaceous formations, GRS therefore performs experiments at URL Mont Terri. Figure 1 shows a sketch overview of selected GRS in situ measurements within the experiments HG-C/BET[i] and EZ-G/WS-H[ii] at URL Mont Terri.

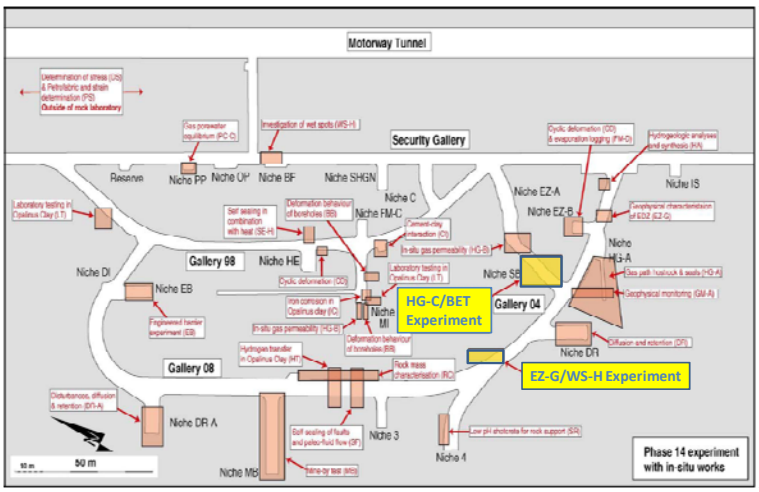

Figure 1: Overview of selected in situ measurements at URL Mont Terri in which GRS is involved

Within the interpretation process, 2D and 3D numerical modeling work, reflecting the actual properties of the rock in situ, is performed and the simulation results are compared to the experimental findings.

2 PHYSICAL MODELING AND NUMERICAL SIMULATION

For reliable physical modeling and numerical simulation the applied constitutive model must be able to represent the test itself (e.g. increase in pore and/or packer pressure) as well as the corresponding behavior of the surrounding rock mass as a consequence of the impact on the initial boundary conditions (e.g. slightly decrease of pore and/or packer pressure down to initial values after the test procedure).

2.1 Physical modeling

In the framework of the presented modeling exercise the computer code CODE_BRIGHT developed by UPC is used for 2D and 3D analysis of coupled hydro-mechanical (HM) phenomena in geological media. Details about the basic theories with the formulated governing equations (balance equations, constitutive models and equilibrium relationships) are described in the code manual[iii]. Regarding the tight coupling between fluid flow processes and mechanical deformation in argillaceous rock mass a simplified approach of the recently developed argillite model[iv] is used, taking into account the anisotropic primary stress field without any damaging process as well as anisotropic mechanical and hydraulic response in case of 3D modeling. The values of the parameters of the investigated Opalinus clay associated with the constitutive model are published in a recent GRS report[v].

2.2 2D-simulation results

On one hand changes in pore pressure could be imposed by the test layout itself, e.g. fluid injection tests for permeability measurement performed within the HG-C/BET project. Figure 2 shows the test location at the SB niche and the corresponding 2D model.

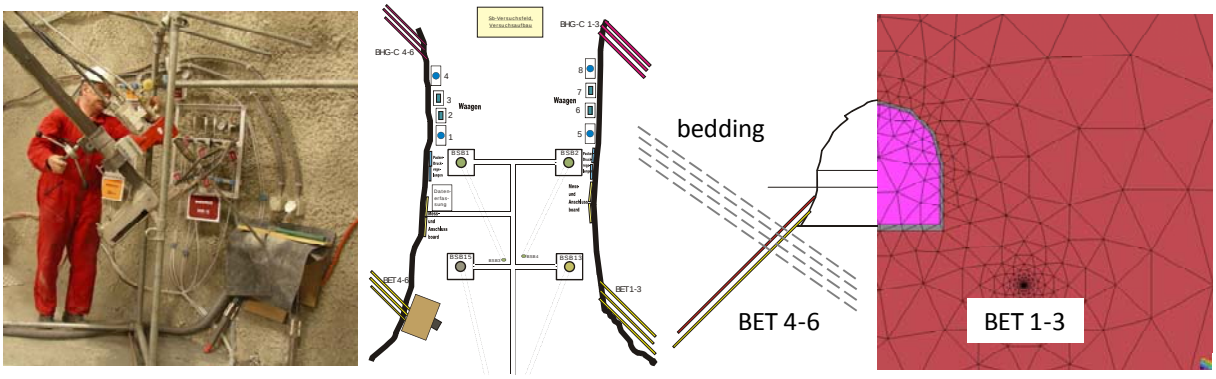

Figure 2: Experimental location at SB niche, borehole drilling process and 2D model used for modeling of fluid permeability measurements in boreholes BET-1 to BET-6

Figure 3 gives an impression on fluid permeability measurements in borehole BET-4-6 (above). While sensor BET-6 shows an elevated pore pressure which is also expected for the undisturbed rock mass, the other two sensors drop below atmospheric pressure after the injection tests. With respect to the experimental findings the numerical results (below) show that considering the ventilation process of the drift cross section over a total time span of

2 years (time between niche excavation and sensor installation) could lead to the observed desaturation of the surrounding rock mass.

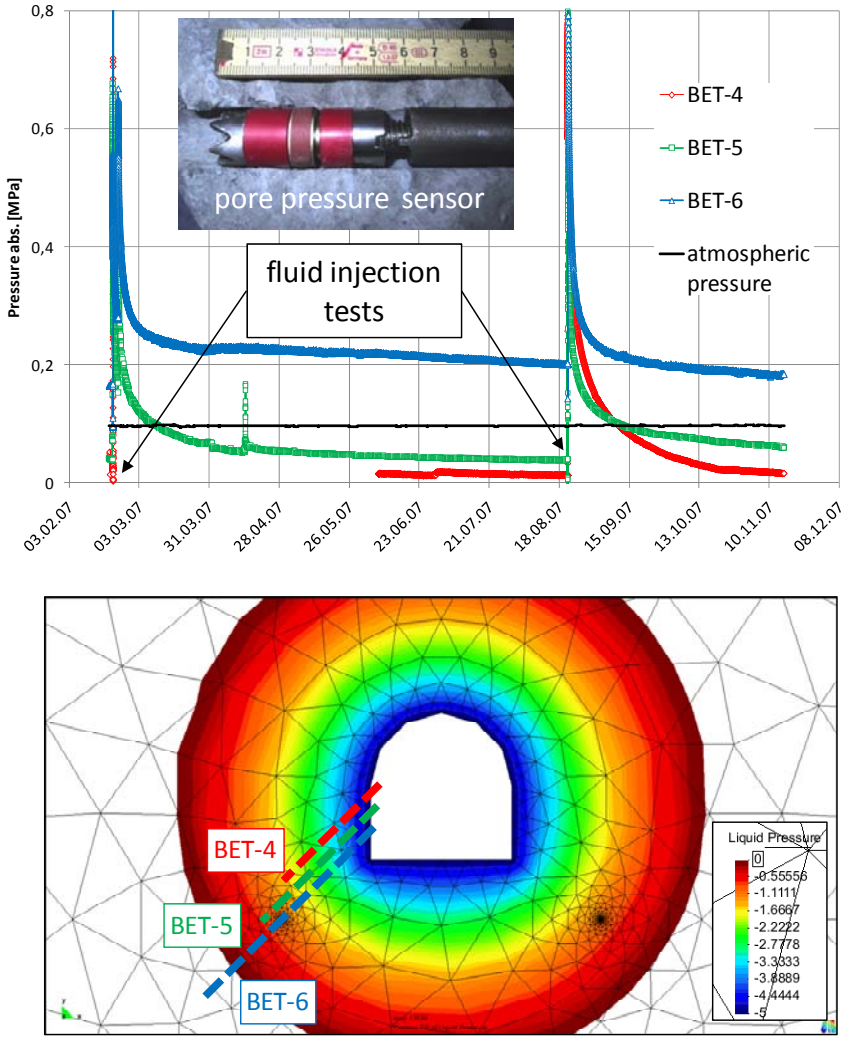

Figure 3: Experimental findings of fluid permeability measurements in boreholes BET-4-6 (above) and numerical results for negative pore pressure values (below)

2.3 3D-simulation results

On the other hand it is obvious that fluid flow processes are related to degradation of pore pressures induced by volumetric deformation due to mechanical loading. Figure 4 shows hydro-mechanical coupled calculation results from 3D-modeling of excavation activities of Gallery 08 compared to pore pressure measurement results at EZ-G niche.

With respect to the experimental findings the numerical results show generally an adequate agreement within the considered borehole measurements. It is obvious when regarding the pore pressure field shown in Figure 3 that the minor distance of borehole BEZ-G6 to the drift floor leads to negative pore pressure values in principle after drift excavation. These values can not be detected by the installed measuring technique. Therefore Figure 4 shows pore pressure values near to atmospheric pressure for the time the excavation front passes sensor BEZ-G6.

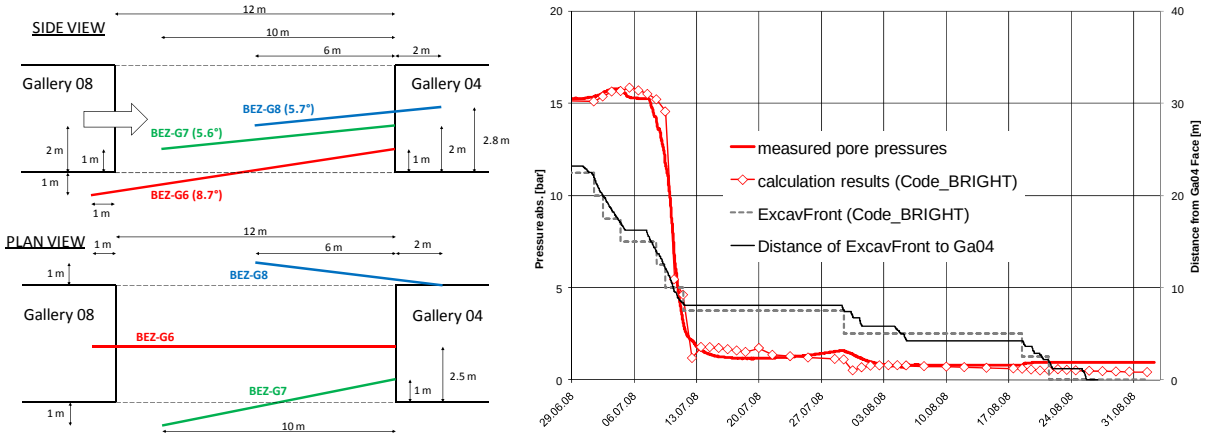

Figure 4: 3D calculation results compared to experimental findings of pore pressure measurements in borehole BEZ-G6 at EZ-G niche

The results for BEZ-G7 and BEZ-G8 (not shown in Figure 4) agree less well. Modeling still needs refinement which is currently in preparation.

3 CONCLUSIONS

The simplified approach of the recently developed argillite model is in principle able to describe the tight coupling between fluid flow processes and mechanical deformation in argillaceous rock mass. Regarding the modeling results for the pore pressure sensors that agree less well to the experimental findings the applied constitutive model may need to be improved with regard to adequate modeling of damage and self-sealing processes and induced permeability changes.

With respect to today's demand for coupling of THMC-processes, there is a lot of work that needs to be done on validating the forecasting tools which are applied for physical modeling and numerical simulation. Further work will be done within the framework of the EC project PEBS.

4 ACKNOWLEDGEMENTS

The authors gratefully acknowledge the funding by the German Ministry of Economics and Technology (BMWi) under contract no. 02 E 10116 and 02 E 10337.

REFERENCES

[i] Miehe, R.,Wieczorek, K., Czaikowski, O., 2010. Barriereintegrität des einschlusswirksamen Gebirgsbereichs in Tonformationen (BET). Abschlussbericht 02 E 10116, in preparation

[ii] Wieczorek, K., Czaikowski, O., 2010. Hydraulic measurements and interpretative modeling in the frame of the Gallery 08 excavation at URL Mont Terri. Technical Report, in preparation

[iii] CODE_BRIGHT, 2002. A 3D program for thermo-hydro-mechanical analysis in geological media. Users guide

[iv] Vaunat, J., 2009. CODE_BRIGHT damage model for argillaceous rocks. CODE_BRIGHT seminar, GRS Braunschweig

[v] Zhang, C.-L., Rothfuchs, T., Dittrich, J., Müller, J., 2008. Investigations on Self-Sealing of Indurated Clay. GRS-230

LARGE SCALE GAS INJECTION TEST (LASGIT) MODELLING

D.Arnedo, S.Olivella and E.E. Alonso

Department of Geotechnical Engineering and Geosciences
Technical University of Catalonia (UPC)
Campus Norte UPC, 08034 Barcelona, Spain
e-mail: diego.arnedo@.upc.edu

Key words: large scale test, gas migration, bentonite barrier

Abstract. *With the objective of understanding the gas flow processes through clay barriers in schemes of radiaoactive waste disposal, the Lasgit in situ experiment was planned and is currently in progress at the Aspö Hard Rock Laboratory. A 3D hydro-mechanical numerical model of the experiment is presented. The materials considered in the simulation are the MX-80 bentonite blocks, the concrete plug and the interfaces between the different materials, which are believed to be a potential preferential path for gas migration through the buffer. The following stages of the experiment are simulated: construction of the isolation barrier inside the deposition hole, Hydration stage 1, Hydraulic test 1 and Gas injection test 1.*

1 INTRODUCTION

The in situ large scale injection test Lasgit is currently being performed at the Aspö Hard Rock Laboratory by SKB and BGS [i]. A schematic layout of the test is shown in figure 1. The deposition hole follows the KBS3 scheme. A copper canister is installed in the axe of the deposition hole, surrounded by blocks of highly compacted MX-80 bentonite. A concrete plug is placed at the top of the buffer. A metallic lid anchored to the surrounding host rock is included in order to prevent vertical movements of the whole system during gas injection stages (high gas injection pressures are expected to be reached). Hydration of the buffer material is achieved by injecting water through filter mats, two placed at the rock walls and two at the interfaces between bentonite blocks. Water is also injected through the 12 canister filters. Gas injection stages are performed injecting gas to some of the canister injection filters.

2 NUMERICAL MODEL

A 3D hydro-mechanical numerical model of the test using CODE_BRIGHT [ii] is presented. The domain considered for the modelling and the different materials are shown in figure 1. The simulation domain corresponds to 1/4 of the deposition hole. The horizontal interfaces between the bentonite blocks and the vertical interfaces corresponding to the host rock and the canister walls contacts are taken into account. Interfaces are believed to be a potential preferential path for gas migration through the buffer. The host rock and the canister are not included in the model due to its high stiffness with respect to bentonite.

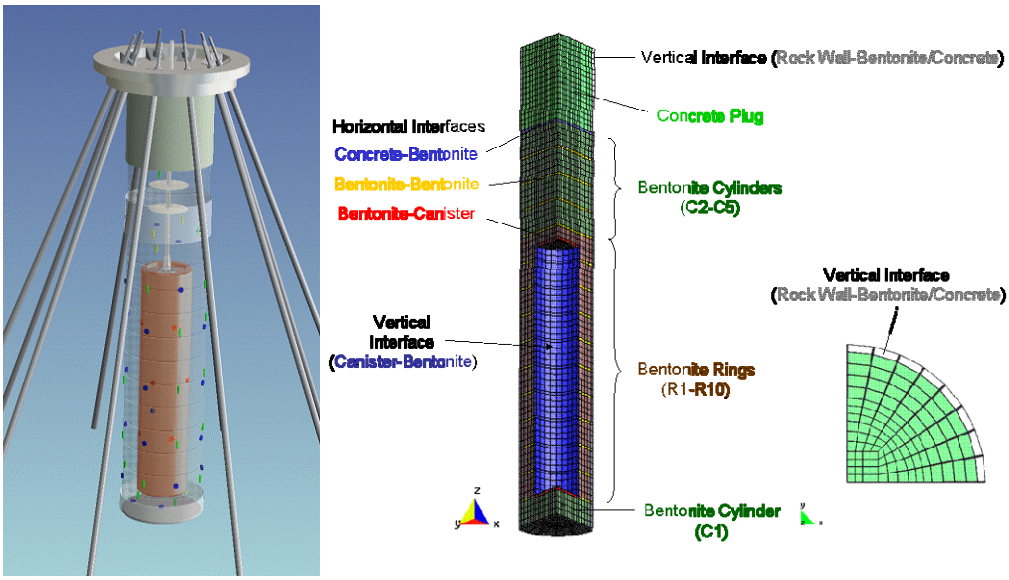

Figure 1. Left: Layout of the Lasgit experiment showing the copper canister with the injection filters (red dots), the bentonite buffer, the location of the filter mats (grey) used for the buffer hydration and some of the instrumentation, the concrete plug and rock anchors. Right: 3D model geometry with the different materials considered in the simulations.

Figure 2 shows schemes of hydraulic boundary conditions (liquid pressure applied at filter mats and injection filters; sinks for gas and water). The position of sinks has been derived from the geological mapping (fractures) of the deposition hole wall made prior to the construction of the isolation barrier.

An elasto-viscoplastic mechanical model based on BBM [iii] is considered for MX-80 bentonite blocks. Non-linear elasticity is used for all interfaces. The concrete plug is linear elastic. Intial permeability of the buffer is $5 \cdot 10^{-20} m^2$. Permeability is one order of magnitude higher along the direction of interfaces. Permeability variations are given by variations of porosity through Kozeny's law.

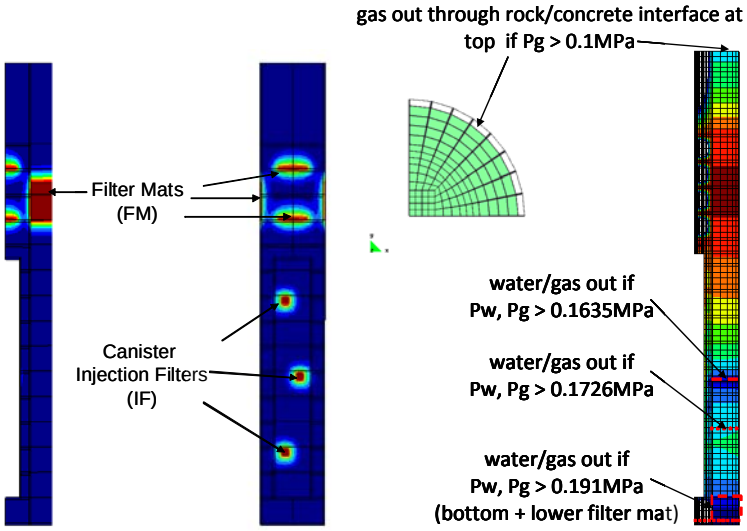

Figure 2. Mechanical and hydraulic boundary conditions.

3 SIMULATION OF HYDRATION STAGE 1

In the numerical model, hydration stage 1 starts at day 10 and ends at day 747. Water pressure is increased at the filter mats to 1.5MPa, which is reached at day 73. From day 561 to day 570 water pressure is increased to 2.35MPa. Figure 3 shows the evolution of saturation degree and liquid pressure during the hydration stage 1. At the end of this stage, the vertical interface between the canister and the buffer, as well as some of the lower horizontal interfaces, remain unsaturated. The lower part of the buffer remains with suction. Fully saturation is not achieved within the bentonite blocks (initial degree of saturation is 0.93)

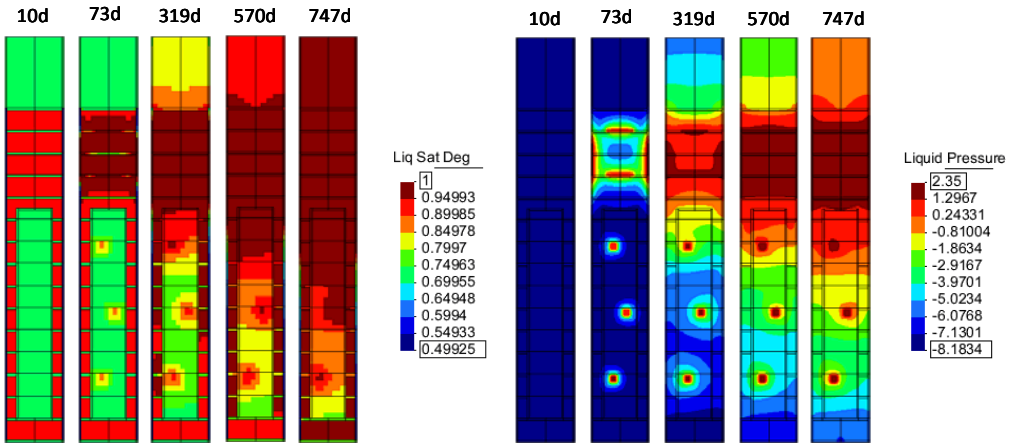

Figure 3. Evolution of saturation degree and liquid pressure. Hydration stage 1.

4 SIMULATION OF GAS INJECTION TEST 1

The gas injection at the lower filter is performed in three stages. First a gas mass flow ramp is applied from 0 to 10^{-6}kg/s during 13 days (day 821 to day 834). Then the gas pressure is prescribed to 1.9MPa during 23 days. Finally gas mass flow is prescribed to 10^{-5}kg/s until the end of the simulation.

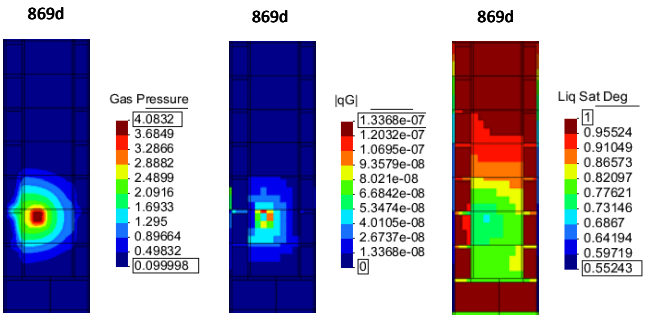

Figure 4. Final fields of gas pressure, gas fluxes and saturation degree. Day 869. Gas injection test 1.

Figure 4 shows the final field of gas pressure, gas fluxes and saturation degree in the lower part of the domain. Gas flows through vertical interface (canister) and mainly through

horizontal interface between bentonite rings towards the sinks at the rock wall contact. Figure 5 shows the initial and final fields of porosity, volumetric plastic strains and major principal stress. An increase of porosity is computed in the vicinity of the lower injection filter. Plastic deformations are obtained in the surrounding bentonite cylinders.

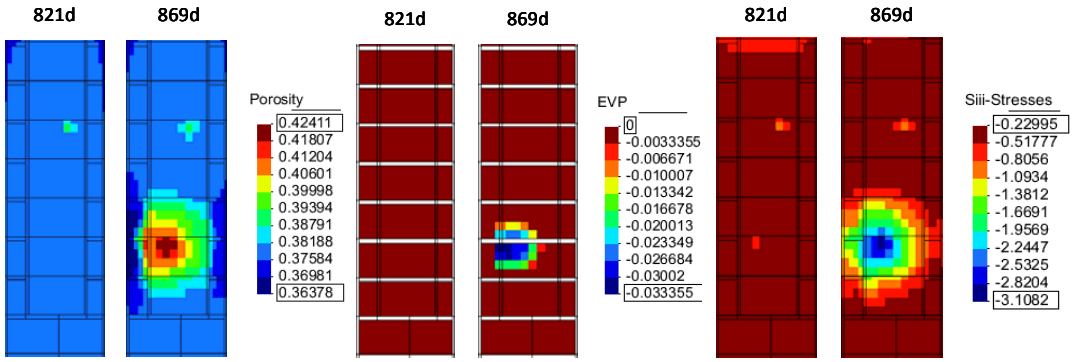

Figure 5. Initial and final fields of porosity, volumetric plastic strains and major principal stress. Gas injection test 1.

5 CONCLUSIONS

A 3D hydro-mechanical model for the large scale gas injection test Lasgit has been presented. The materials considered are the MX-80 bentonite blocks of the isolation barrier and the different interfaces between materials. The simulation includes the following stages of the test: construction of the deposition hole, hydration stage 1, hydraulic test 1 and gas injection test 1. Initial results show that full saturation is not achieved within the lower bentonite blocks and that some of the lower interfaces, especially the vertical interface between the clay blocks and the canister, remain unsaturated. During gas injection stage the gas flows through the interfaces near the injection filter and moves mainly through the horizontal interface towards the sinks representing the fractures at the rock wall.

6 REFERENCES

[i] Sellin, P., J.Harrington, 2006, 'Large-scale gas injection test (Lasgit) - current status', Proc. . 11th International High Level Waste Management Conference, IHLRWM, pp: 792-797.

[ii] Olivella, S., A. Gens, J. Carrera, E. E. Alonso, 1996, 'Numerical Formulation for a Simulator (CODE_BRIGHT) for the Coupled Analysis of Saline Media', Engineering Computations, Vol 13, No 7, pp: 87-112.

[iii] Alonso, E.E., A. Gens, A. Josa, 1990, 'A constitutive model for partially saturated soils', Géotechnique, 40(3): 405-430.

MODELLING EARTH DAM CONSTRUCTION AND LONG TERM RESPONSE

Sebastià Olivella, Núria Pinyol and Eduardo Alonso
Department of Geotechnical Engineering and Geosciences

Abstract: *This paper describes capabilities of CODE_BRIGHT–GiD to analyze construction and long term response of earth dams. The paper focuses in the construction process of earth dams and related aspects and highlights the complexity of the boundary conditions to be applied in these problems.*

1. INTRODUCTION

The program CODE_BRIGHT couples the thermal (multiphase heat transport in porous media), hydraulic (two phase flow of liquid and gas in porous media), mechanical (unsaturated soil mechanics) problems and the solute transport. These problems require a number of constitutive laws and these have been organized accordingly. Since the number of material properties and parameters is large, it is useful to import sets of parameters if they are similar in other applications.

A functionality that was introduced in CODE_BRIGHT is the construction and excavation of geomaterials. This is of especial relevance in geotechnics as most of problems require construction (for example an earth dam or and embankment) or excavation (for example tunneling and diaphragm walls). From the finite element point of view, this facility implies activation and deactivation of elements, typically by layers. Normally, ramp variation of weight application permits to fully smooth this process which is very important for avoiding sharp changes which may lead to numerical difficulties and do not correspond to the actual process in the field. In the case of GiD pre-process this is solved by combination of material definition by layers which activate and deactivate in the different intervals. Yet, construction or excavation implies change of boundary condition position. For instance, the atmospheric conditions (rain and evaporation at soil surface) move as soil layers are constructed in an embankment. Applications of earth dam construction are presented to illustrate the capabilities of the program.

2. BELICHE DAM

Figure 1 shows an earth dam which was constructed in Algarve (Portugal) using rockfill and clay. This earth dam was extensively monitorized in terms of displacements, pressures and stresses. Alonso, Olivella and Pinyol (2005) present a review which includes geotechnical analysis of the dam behaviour taking into account construction stages, water level rise in the reservoir and long term behaviour during different rainfall events. The constitutive models used in that contribution (Rockfill Model and Barcelona Basic Model) have been integrated using a viscoplastic approach and are the more advanced framework existing in the field of geotechnics of earth dams. This problem is used in this paper to discuss different aspects that are related to the modelling performed.

Material Parameters

The material parameters in this problem consist in hydraulic parameters and mechanical parameters. The hydraulic parameters are hydraulic conductivity, retention curve (water content versus capillary pressure) and relative permeability. All are nonlinear functions. The mechanical parameters correspond to a generalized viscoplastic model for unsaturated soils and rockfills, based on Perzyna theory. Flow rule, failure envelope and compression parameters are different for the clay core and for the rockfill shoulders. A total of 15 parameters are required for each material (clay core, inner rockfill, outer rockfill). Hence, the existing possibility in GiD to import and export a material is obviously extremely useful as permits to transfer sets of parameters from one problem to another. In principle, history variables (such as preconsolidation stress) are required as a function of space, however if construction is simulated, these history variables can be set constant by surfaces or volumes, or by materials.

Beliche dam (Algarve, Portugal)

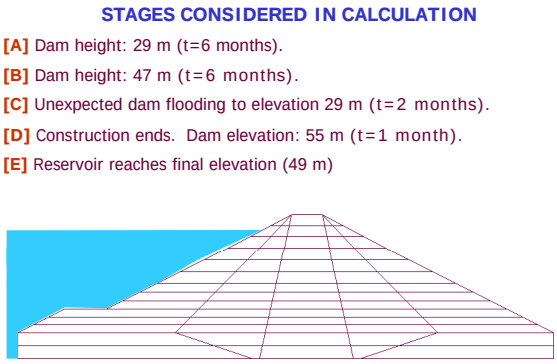

Intervals included during the analysis

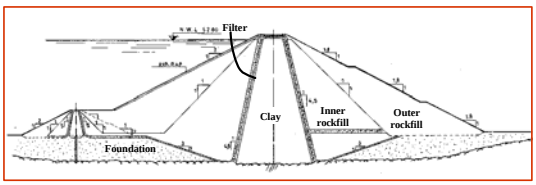

Materials

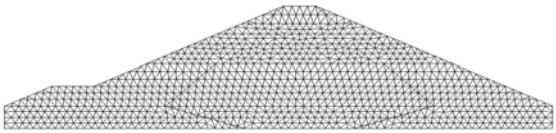

Finite element mesh made of quadratic triangles

Figure 1. Modelling an earth dam (rockfill shoulders + clay core). (from Alonso, Pinyol and Olivella, 2005).

Construction intervals

The stress state in a geotechnical structure such as an earth dam can only be determined if the construction is simulated realistically. In this problem, construction was simulated by layers (these are indicated in Figure 1). In CODE_BRIGHT, materials and construction layers are identified, and therefore a number of materials have to be defined in this case. However, any new material can be defined as having the same properties as an existing one. For instance, any new layer of soil has the same properties as the ones already constructed but the material is still in its soft state (hardening history variables have not yet changed because they are element dependent). Even construction using thin layers may be a numerical problem if the loading is instantaneous. Therefore, in order to smooth the construction process, the final weight of each layer is achieved in a ramp way during the time interval. Since the material is soft during construction, the self weight and the progressive construction of subsequent layers implies a hardening of the material which is realistic. In CODE_BRIGHT, a material may have 3 states: (a) active, (b) is constructed during the interval and (2) not active (has been excavated or

not yet constructed). Construction of each layer is done during specified time periods (intervals).

Boundary conditions

The problem of the earth dam described in figure 1 requires several boundary conditions. The earth layers that are constructed are exposed to the atmosphere and hence, rain and relative humidity (suction in this case) should be prescribed during time. Since the exposed surface to the atmosphere in the earth dam changes with time, the boundary condition should change with space and time. The boundary conditions applied to unconstructed layers are not active until the layers are constructed. As a new layer is constructed the boundary conditions should disappear. Figure 2 shows the rainfall evolution and dam water level in the reservoir that were applied as boundary conditions. The response in terms of water pressure in the dam (time evolution plot and contour field plots) shows that transient conditions prevail due to continuous changes in boundary conditions. Upstream and downstream points undergo different response due to water level in the reservoir, but the downstream points reach liquid pressures close to zero.

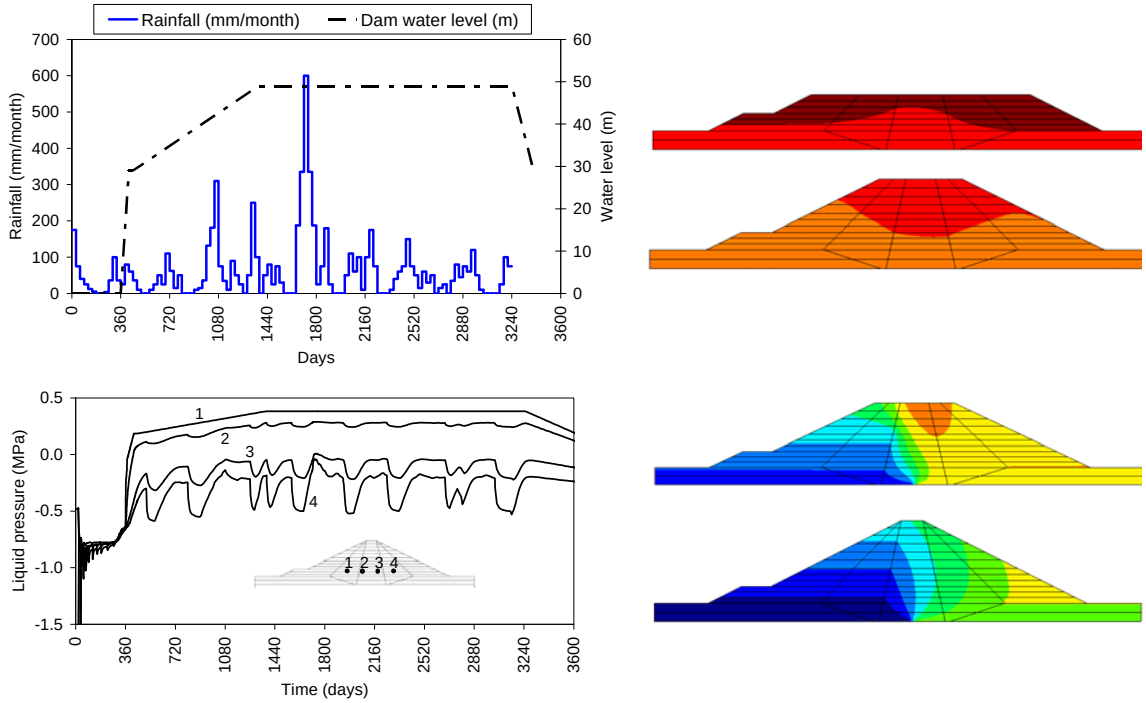

Figure 2. Evolution of rainfall and water level in the reservoir and response of liquid pressure in the dam (Alonso, Olivella and Pinyol, 2005).

The impounding history of the reservoir is simulated by means of a set of periods in which the water level changes linearly between the two extreme times (t_a, t_b) considered. To this end, the auxiliary function:

$$p(t) = \frac{t - t_b}{t_a - t_b} \quad \text{for} \quad t_a < t \le t_b \tag{1}$$

is introduced. Water pressure at a point of the boundary having a vertical height, y, above the reference level, is given by:

$$p_w = \gamma_w h(t) \tag{2}$$

where

$$h(t) = H \times p(t) - y \qquad \text{if} \quad H \times p(t) > y$$
$$h(t) = 0 \qquad\qquad \text{if} \quad H \times p(t) \le y \tag{3}$$

where H is the maximum reservoir level in the period considered. Normal stresses on the upstream boundary are specified equal to the liquid water pressure:

$$\sigma_n = p_w \tag{4}$$

Alternatively, the water in the reservoir can be represented explicitly as a material with appropriate parameters equivalent to water properties. If this material can undergo the two states, namely dry and fully saturated, then the water level variations can be represented adequately.

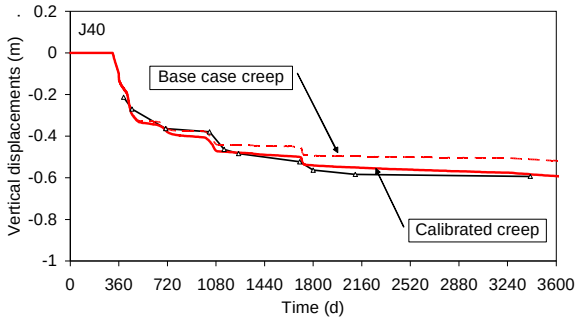

Displacements measured and calculated at a point near the crest of the dam.

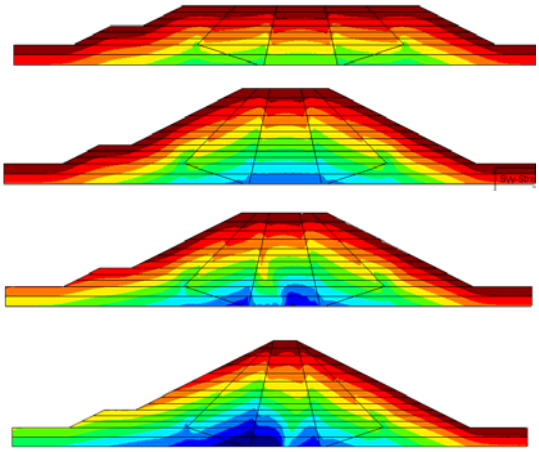

Figure 3. Evolution of displacements and vertical stress distribution (Alonso, Olivella and Pinyol, 2005).

Finally, Figure 3 shows the results of displacements (evolutions) and stresses (distribution at different stages of the model) in the earth dam. The displacements are compared with measurements that were recorded during several years. Note that the discplacement increase around 1800 days is related with a peak in the water pressure curve (Figure 3). This is due to a collapse deformation induced by impoundment that takes place in the clay core and the rockfill shoulders. Intensity and duration of rainfall events play a major role in the earth dam long term behavior. Stress distribution is quite sensitive to collapse, as the collapsing zones undergo unloading while the zones that remain more stiff undergo loading.

3. CONCLUDING REMARKS

More recently, new attempts to model the response of other dams have been undertaken. The experience from Beliche Dam modeling is very important for further efforts in this direction. Yet, there are several aspects to be improved like for instance reservoir boundary condition, smoothing of displacement field for constructed layers and automatic application of rain and evaporation during construction.

4. REFERENCES

Alonso, E., S. Olivella, N-M. Pinyol (2005). A review of Beliche dam. *Géotechnique*, 55(4): 267-285.

PARAMETRIC STUDY ON COMPACTION CONDITION OF THE CORE IN THE BEHAVIOUR OF A ZONED EARTH DAM

Lícia Mouta da Costa[1] and Eduardo Alonso[2]

[1] Civil Engineering Department
Federal University of Pernambuco
Av. Acadêmico Hélio Ramos, s/n, 50740-530,Recife-PE – Brazil
e-mail: licia@ufpe.br

[2] Department of Geotechnical Engineering and Geosciences
Technical University of Catalonia (UPC)
Módulo D2, Campus Nord, c/ Jordi Girona, 1-3, 08034 Barcelona, Spain
e-mail: eduardo.alonso@upc.edu

Key words: compaction conditions, earth dam, hydro-mechanical coupled analysis

Abstract. *This paper presents a parametric study performed to evaluate the effects of the compaction water content of the core material on the behavior of a zoned earth dam. A coupled hydro-mechanical formulation implemented in CODE_BRIGHT was applied to simulate the construction of a zoned earth dam. The constitutive model adopted for the mechanical behavior of the shoulder, filter and core materials is the Barcelona Basic Model (BBM)[(1)] for unsaturated materials. The hydraulic behavior is described by water retention characteristics and the permeabilities, which is expressed as a function of porosity and degree of saturation.*

1 INTRODUCTION

Compaction states are defined in practice by the dry specific weight (γ_d) and the water content (w). Properties of compacted soils are expected to change when the pair (γ_d, w) changes. Unsaturated soil mechanics offer a powerful alternative to estimate the properties of compacted soils. Considering the constitutive model BBM[(1)], the pair (γ_d, w) could be substituted by the pair (p_0^* , s)[(2)].

The purpose of this paper is to predict the core behaviour for three different compaction conditions. The assumption is that the dry density is maintained and the compaction water content changes (from dry to wet conditions).

2 NUMERICAL SIMULATION

The analysis carried out simulated the construction of Lechago dam, as defined in the design. The dam presents a central compacted clay core, protected by granular filters and wide rockfill shoulders. A representative cross section of Lechago dam is given in Figure 1a. Figure 1b shows the finite element mesh used (1077 triangular elements and 487 nodes). A total of nine horizontal layers whose thickness varies between 3 and 6 m were defined. Construction or excavation is simulated by "switching" on or off a set of elements.

The lower boundary of the discretization is assumed to be fixed and impervious. Upstream and downstream ends of the foundation layers are also restrained to move in a horizontal direction and are considered impervious. Initial conditions for foundation elements are

simple: a geostatic total stress distribution and a hydrostatic water pressure. Built elements are assigned a small arbitrary initial stress to avoid instabilities in the nonlinear constitutive equations. For filter and rockfill elements initial suction was taken as 0.05 MPa. Given the low value of the air entry value for these coarse granular materials, this initial suction results in a very low saturation. Material properties were determined from a series of laboratory tests carried out[3].

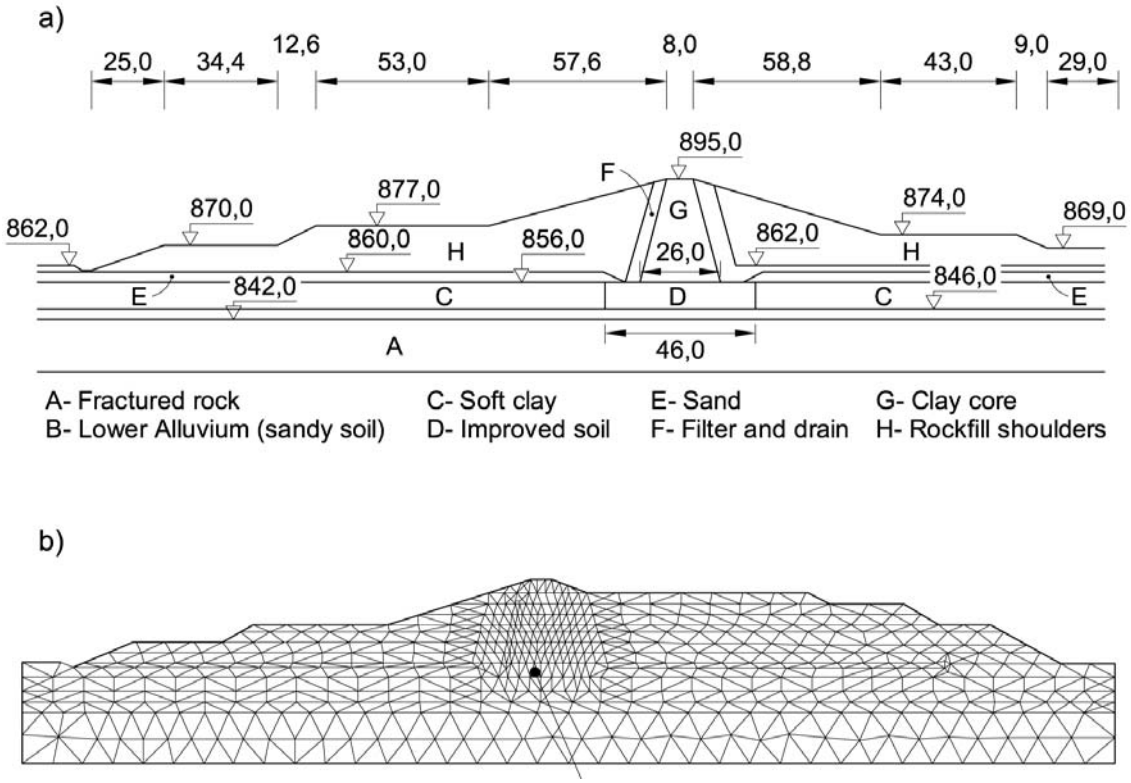

Figure 1: a) Cross section of Lechago dam; b) Finite element mesh for dam construction

In order to verify the influence of compaction water content, three conditions were analyzed: (a) dry of the optimum, (b) optimum +2.7% and (c) wet of the optimum. Table 1 specifies the assumed initial suctions for these conditions, as well as the degree of saturation derived from the water retention relationship.

Compaction condition	S_{l0} (%)	s_0 (MPa)
Dry core	55	15.0
Core at $w_{opt.+2.7\%}$	75	3.0
Wet core	90	0.8

Table 1 : Initial conditions for the parametric study on compaction conditions

Figure 2 presents the distribution of degree of saturation in the core at the end of construction for the three conditions. The wet core becomes almost saturated at the end of construction. However, positive pore pressures develop only in the lower part of the core (Figure 3). Small negative pressures (within the range of the air entry value in most of the core) are calculated. The core loses water towards the rockfill shoulders in the cases solved. At the end of construction the dry core maintains degrees of saturation - in the range 0.6 (upper part) to 0.9 (lower part) and high suctions.

Changes of degree of saturation and pore pressure are always controlled by the specific shape of the water retention curve. These two variables are always located on the water retention curve. It is also interesting to realize the coupled nature of phenomena since changes in degree of saturation affect directly the permeability, which in turn, controls the distribution of water pressures.

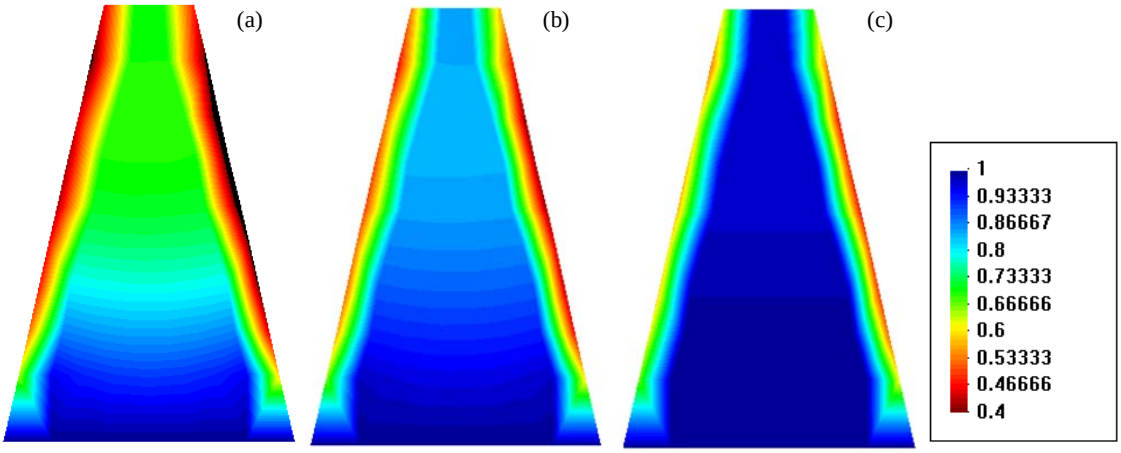

Figure 2: Distribution of degree of saturation in the core at the end of construction: (a) Dry core; (b) Core at wopt.+2,7%; (c) Wet core.

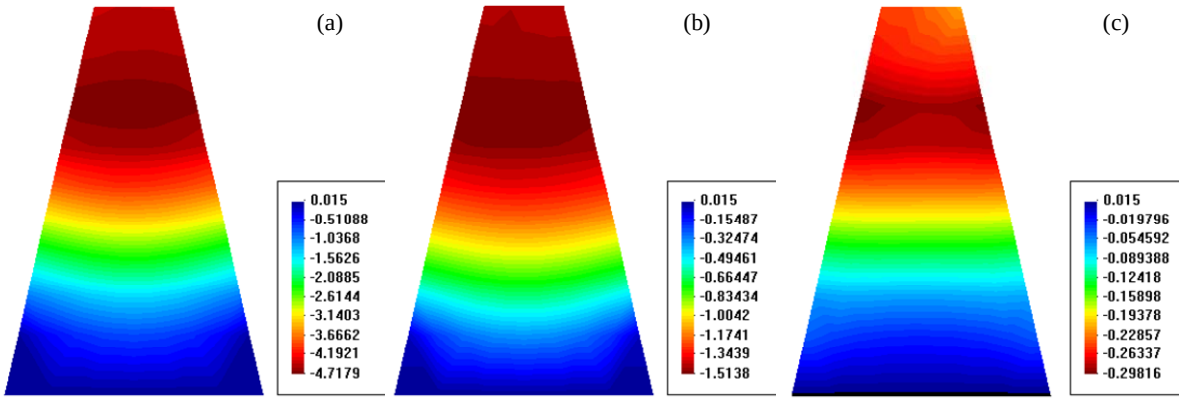

Figure 3: Distribution of pore water pressure in the core at the end of construction: (a) Dry core; (b) Core at wopt.+2,7%; (c) Wet core.

Figure 4 shows the distribution of vertical settlements along the dam axis at the end of construction for the three compaction conditions. Higher settlements are calculated for the wet core, which presents the maximum at a higher height than the two other cases. This is explained because the lower suctions associated with wet conditions imply a higher compressibility and a lower yielding stress.

The influence of compaction water content in the development of the arching effect is presented in Figure 5. The wet core is more deformable and the stress transfer mechanism is more pronounced. On the other hand the dry core is more rigid and the arching effect is less developed.

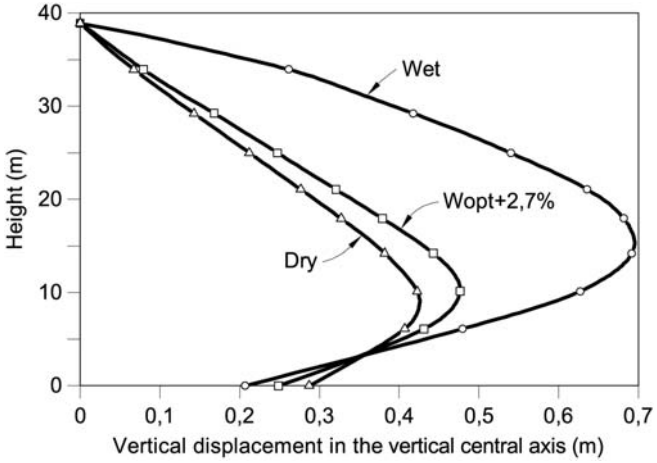

Figure 4: Vertical displacement distribution in the central axis at the end of construction.

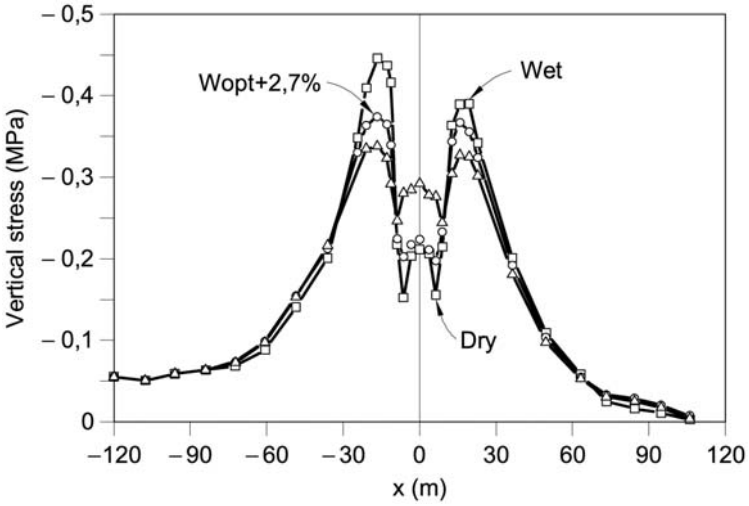

Figure 5: Vertical stress in the horizontal section AB at the end of construction.

3 CONCLUSIONS

Simulation of dam construction shows the influence of suction in soil strength and stiffness. Changes in degree of saturation and water pressure pointed out how relevant are the water retention curve and non linear variation of permeability.

The analysis presented indicated that the core compacted at the dry of the optimum water content is more rigid, stress transfer is less pronounced and foundation differential settlements are smaller. On the other hand, considerable suction values remain at the end of construction.

REFERENCES

[1] Alonso, E.E., Gens, A. and Josa, A. (1990). A constitutive model for partially saturated soils, Géotechnique, 40, 3, 405-430.

[2] Alonso, E.E., and Pinyol, N.M. (2008). Unsaturated soil Mechanics in earth and rockfill dam engineering. Opening Lecture. Proceedings of the 1st European Conference on Unsaturated Soils, Durham, UK. 3-32.

[3] Costa, L. M. da (2000). Análise hidro-mecânica de solos não saturados com aplicação a barragem de terra. Doctoral thesis, COPPE/UFRJ, Rio de Janeiro.

TWO MODIFICATIONS OF CODE_BRIGHT-BBM TO FACILITATE THE REPRESENTATION OF BENTONITE CLAY

Ola Kristensson [*] **and Mattias Åkesson** [*]

[*] Clay Technology AB
IDEON Research Center
S-223 70 Lund, Sweden
e-mail: osk@claytech.se

Key words: Continuum mechanics, Constitutive modeling, BBM, Bentonite

Abstract. *Two modifications of the thermoelastoplastic constitutive law (based on BBM) available in Code_Bright have been developed and implemented. The modifications are made to facilitate the mechanical representation of bentonite clay. The first modification addresses the swelling modulus and the second addresses the slope of the critical state line. The modifications are used in some simple test cases and are found to be beneficial when representing bentonite clay behaviour.*

1 INTRODUCTION

In simulations of the Swedish KBS-3 concept for a nuclear waste repository the homogenization of the engineered clay buffer when swelling due to water uptake is addressed. Presently, the thermoelastoplastic model in Code_Bright, based on BBM, is used to represent the bentonite clay in the engineered buffer. It has however been found that some of the characteristic behaviors, found experimentally, are hard to mimic with the existing formulation of the material model. In order to meet experimental findings, two of the phenomenological relations, concerning the swelling pressure and failure stress, are incorporated in the theoretical framework.

2 SWELLING MODULUS DEPENDENT ON SWELLING PRESSURE CURVES

A new function governing the swelling modulus κ_s in BBM has been implemented in Code Bright in order to mimic the behavior of bentonite clay. The idea behind the new expression is to utilize a swelling pressure curve (the pressure obtained at full water saturation under confined conditions) obtained from analyzing experimental data. The adopted function has following form,

$$\kappa_s(p',e) = \kappa_{s0} f(p',e) \tag{1}.$$

$$f(p',e) = \begin{cases} 1 & \text{if } p' < p_{ref} \\ 10^{-20} & \text{if } p' > p_{swell}(e) \\ 1 - \dfrac{\ln p' - \ln p_{ref}}{\ln(p_{swell}(e)) - \ln p_{ref}} & \text{otherwise} \end{cases}$$

$$p_{swell}(e) = 10^{\left[-4.741+4.117\cdot10^{-3}\frac{\rho_s}{1+e}-3.94\cdot10^{-7}\left(\frac{\rho_s}{1+e}\right)^2\right]}$$

In Figure 1 the pressure dependence of the normalized function (κ_s/κ_{s0}) is shown for two constant void ratios. When the pressure, p', is less than the referential pressure, p_{ref}, the function equals the referential value κ_{s0}. Thus, the upper "knee" occurs when $p = p_{ref}$. When $p = p_{swell}(e)$ the function equals zero (or rather 10^{-20} to avoid division by zero). Thus, swelling may occur until the pressure equals the swelling pressure at the current void ratio.

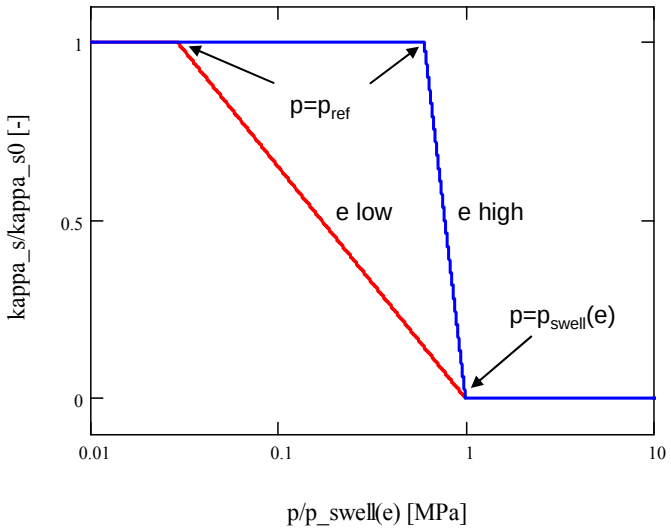

Figure 1: Page layout example

The void ratio dependence is shown in Figure 2 below where the normalized modulus is given for three constant pressures. The void ratio is normalized against the void ratio, e_s, that give the specified pressure when inserted in the swelling pressure function. As can be seen, the modulus decreases with increasing void ratio.

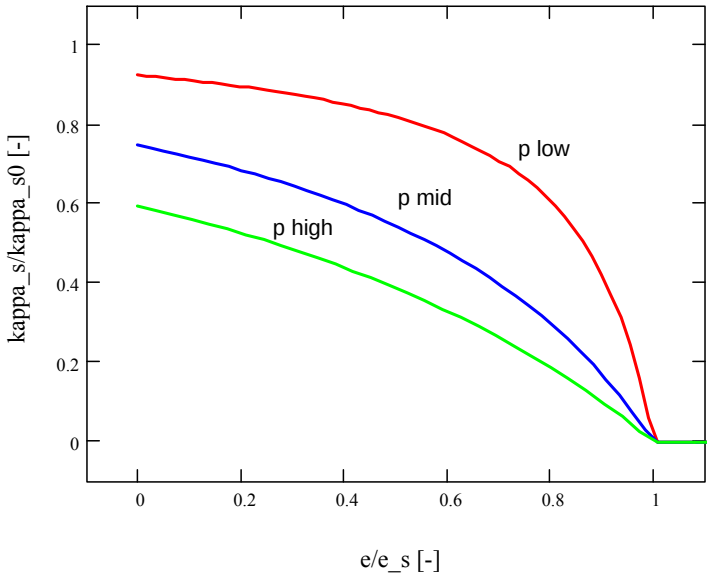

Figure 2 Void ratio dependence of the normalized swelling modulus

Below, some simple elastic and isotropic examples are studied using MathCad. Thus, we

only consider states inside the yield surface that also stay inside the yield surface during wetting. At the higher void ratios used this is probably not a very suitable representation, but this exercise is only performed to study the performance of the modulus-function.

First, wetting under constant pressure is investigated when using the modulus function. The unsaturated clay sample can be thought of being contained within a soft membrane that is subjected to an outer constant pressure p. When water is added to the clay, the specimen should swell until the swelling pressure equals the outer prescribed pressure. In the results shown in Figure 3 below, obtained from using the expression above, it can be seen that the void ratio obtained at full water saturation, e_s, is given by $p_{swell}(e_s) = p$, as expected.

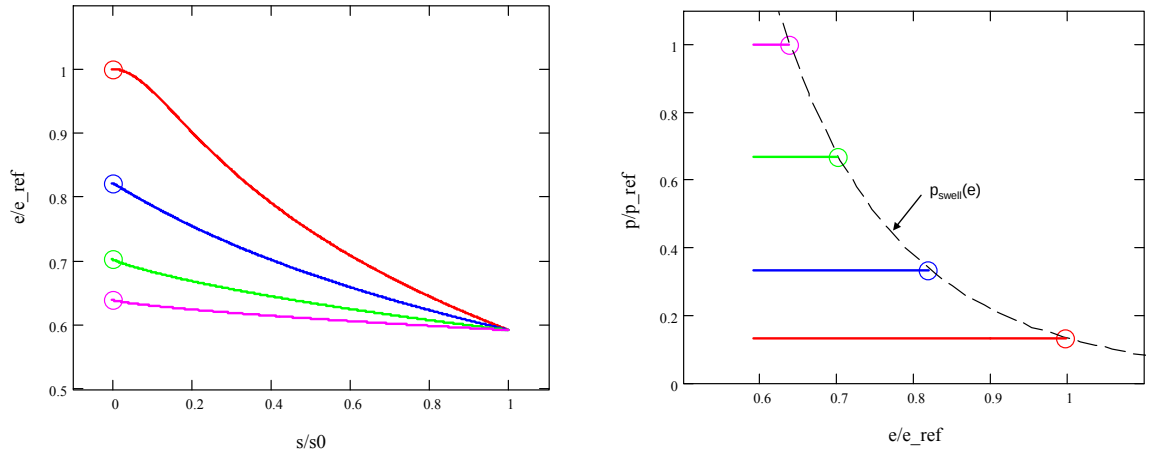

Figure 3 Responses for wetting under constant pressure.

The next simple case we will study is wetting under constant void ratio e (confined swelling). Two different void ratios are used. Here, the final pressure p, at full water saturation, should match the swelling pressure curve so that $p = p_{swell}(e)$. In this example, also the elastic flexibility modulus κ_i in BBM comes into play. For the two different void ratios the parameters in κ_i have been kept the same. As can be seen in Figure 4, the results from using the modulus function follow the adopted swelling pressure curve.

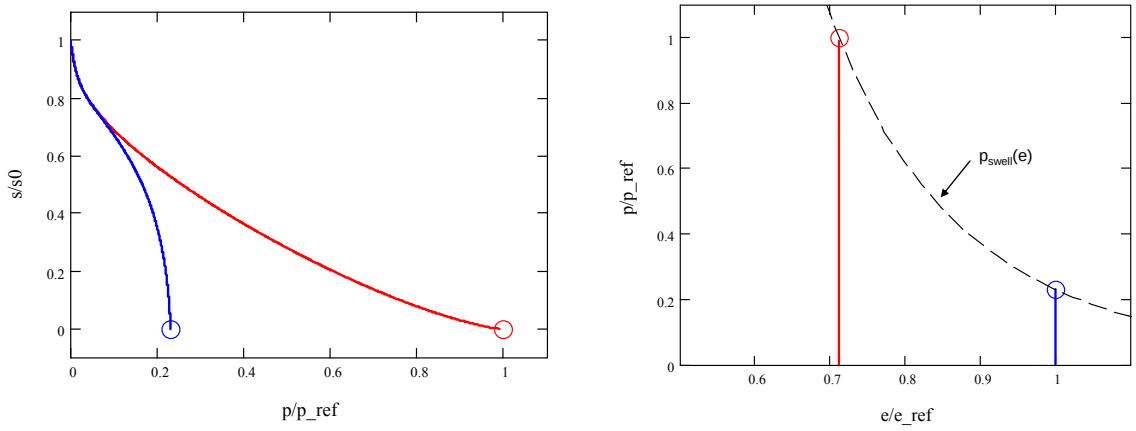

Figure 4 Responses for confined wetting.

3 INCORPORATION OF A VARYING CRITICAL STATE LINE SLOPE PARAMETER IN BBM

The underlying idea with this modification is to incorporate a dependence of M (representing the slope of the critical state line) so that an experimentally validated expression of the type $q_f = q_f(p')$ that are found for bentonite clay are fulfilled.

In BBM the deviatoric failure stress q_f occurs at the mid-point pressure $p'_{mid} = (p_0 - p_s)/2$ of the yield surface f. When failure occurs the material model behaves plastic, i.e. $f = 0$. The obtained expression reads,

$$f = q_f^{\,2} - M^2\left(p'_{mid} + p_s\right)\left(p_0 - p'_{mid}\right) = 0 \tag{2}$$

The parameter M may accordingly be expressed as,

$$M = \frac{q_f(p'_{mid})}{\frac{p_0 + p_s}{2}} \tag{3}$$

The experimentally validated $q_f = q_f(p')$ expression reads,

$$q_f(p') = ap'^{b} \tag{4}$$

, where no cohesion is present. Since p_s describes the cohesion in BBM, the original expression of q_f has been altered to

$$q_f(p') = a(p' + p_s)^b \tag{5}$$

If this altered expression is used in the expression of the variable M we obtain,

$$M(p_0, p_s) = \frac{q_f\left(\frac{p_0 - p_s}{2}\right)}{\frac{p_0 + p_s}{2}} = a\left(\frac{p_0 + p_s}{2}\right)^{b-1} \tag{6}$$

Below the new relation $M = M(p_0, p_s)$ is introduced into the BBM framework and the new contributions are shown. A von Mises type yield surface is considered (meaning that it is independent of Lode's angle) and the temperature dependence is omitted.

The differential of the yield surface becomes,

$$df = \frac{\partial f}{\partial \boldsymbol{\sigma}} \cdot d\boldsymbol{\sigma} + \frac{\partial f}{\partial s} ds + \frac{\partial f}{\partial \varepsilon_v^{\,p}} d\varepsilon_v^{\,p} \tag{7}$$

, where the new dependency of M will have an effect on the last two partial derivatives since $p_0 = p_0(s, \varepsilon_v^p)$ and $p_s = p_s(s)$. The additional contributions can be seen when evaluating the partial derivatives below,

$$\frac{\partial f}{\partial s}=\frac{\partial f}{\partial p_0}\frac{\partial p_0}{\partial s}+\frac{\partial f}{\partial p_s}\frac{\partial p_s}{\partial s}=\left(\left.\frac{\partial f}{\partial p_0}\right|_{dM=0}+\frac{\partial f}{\partial M}\frac{\partial M}{\partial p_0}\right)\frac{\partial p_0}{\partial s}+\left(\left.\frac{\partial f}{\partial p_s}\right|_{dM=0}+\frac{\partial f}{\partial M}\frac{\partial M}{\partial p_s}\right)\frac{\partial p_s}{\partial s} \tag{8}$$

$$\frac{\partial f}{\partial \varepsilon_v^{\,p}}=\frac{\partial f}{\partial p_0}\frac{\partial p_0}{\partial \varepsilon_v^{\,p}}=\left(\left.\frac{\partial f}{\partial p_0}\right|_{dM=0}+\frac{\partial f}{\partial M}\frac{\partial M}{\partial p_0}\right)\frac{\partial p_0}{\partial \varepsilon_v^{\,p}}$$

Since the partial derivatives above now have additional terms, there will be contributions to the elastoplastic stiffness tensors $\boldsymbol{C}^{ep}$ and $\boldsymbol{c}^{ep}$,

$$d\boldsymbol{\sigma}=\boldsymbol{C}^{ep}d\boldsymbol{\varepsilon}+\boldsymbol{c}^{ep}ds \tag{9}$$

$$\boldsymbol{C}^{ep}=\boldsymbol{C}^{e}-\frac{1}{A}\left(\boldsymbol{C}^{e}\frac{\partial g}{\partial \boldsymbol{\sigma}}\right)\otimes\left(\boldsymbol{C}^{e}\frac{\partial f}{\partial \boldsymbol{\sigma}}\right)$$

$$\boldsymbol{c}^{ep}=\boldsymbol{c}^{e}-\frac{1}{A}\frac{\partial f}{\partial s}\boldsymbol{C}^{e}\frac{\partial g}{\partial \boldsymbol{\sigma}}-\frac{1}{A}\frac{1}{3K^{h}}\left(\left(\boldsymbol{C}^{e}\frac{\partial g}{\partial \boldsymbol{\sigma}}\right)\otimes\left(\boldsymbol{C}^{e}\frac{\partial f}{\partial \boldsymbol{\sigma}}\right)\right)\boldsymbol{I}$$

$$A=-\frac{\partial f}{\partial \varepsilon_v^{\,p}}\frac{\partial g}{\partial p'}+\frac{\partial f}{\partial \boldsymbol{\sigma}}\cdot\left(\boldsymbol{C}^{e}\frac{\partial g}{\partial \boldsymbol{\sigma}}\right)$$

The additional terms in (8) are here specified in the variables and parameters used

$$\frac{\partial f}{\partial M}=-2M(p'+p_s)(p_0-p') \tag{10}$$

$$\frac{\partial M}{\partial p_0}=\frac{a(b-1)}{2}\left(\frac{p_0+p_s}{2}\right)^{b-2}$$

$$\frac{\partial M}{\partial p_s}=\frac{a(b-1)}{2}\left(\frac{p_0+p_s}{2}\right)^{b-2}$$

The implementation is tested below for a case where a loose clay specimen is first subjected to an increasing hydrostatic stress state which is followed by a “triaxial test” stress state (shearing), where two of the principal stresses are held constant and the third is increased (compressively). Drained hydraulic conditions prevail during the process. A case with a constant M and the new varying M are used to investigate the differences of the two implementations. The models are solved using Code_Bright.

The shearing is started at two different levels of hydrostatic pressure in order to investigate the behavior of the models for different stress evolutions. λ is set to correspond to the void ratio e at the start of shearing at the higher level of hydrostatic stress. This has been done in order to enable evaluation against the closely related experimental conditions of T17 in TR-95-20. The used swelling pressure curve is utilized for obtaining a value of λ,

$$\lambda(e)=\left[\frac{\mathrm{d}\ln\left(p_{swell}(e)\right)}{\mathrm{d}e}\right]^{-1} \tag{11}$$

$$p_{swell}(e)=10^{\left[-4.741+4.117\cdot10^{-3}\frac{\rho_s}{1+e}-3.94\cdot10^{-7}\left(\frac{\rho_s}{1+e}\right)^2\right]}$$

It should here be mentioned that a third modification has indeed been developed and implemented in the code, where (11) is used for determining λ. When using this implementation however, difficulties with convergence are experienced. If this origins in errors in the implementation or that the formulation in itself is "too sensitive" has not been investigated.

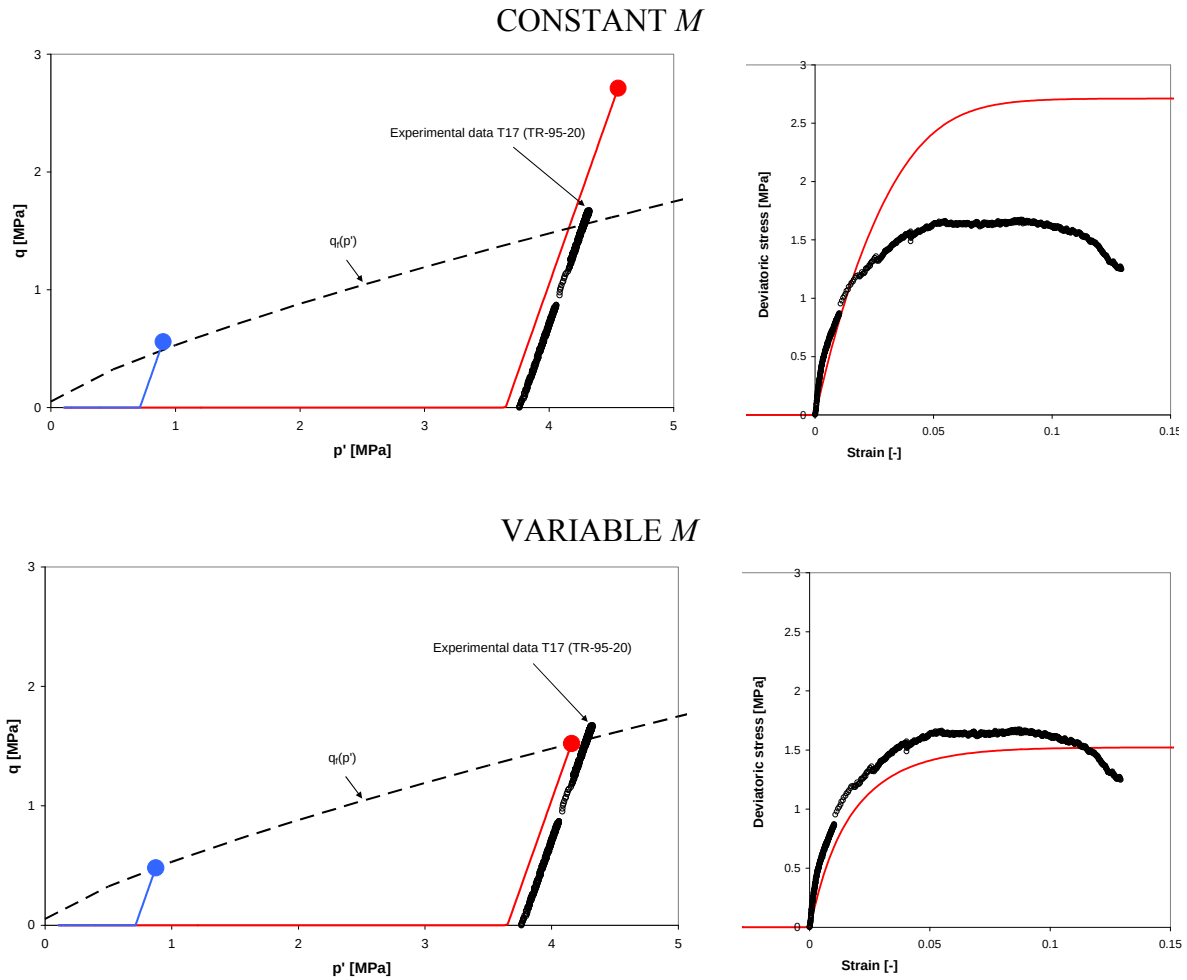

Figure 1 Stress state (left) and q – strain relation (right) for the constant M (top) and variable M (bottom) models.

As can be seen in Figure 1 the responses obtained using the variable M implementation are more in agreement with both the $q_f(p')$ expression as well as the T17 data as compared to the constant M implementation. Still, in order to obtain the nice fit against the experimental stress – strain relation in the right figures a "target void ratio" has to be chosen when determining the elastoplastic flexibility modulus λ.

4 CONCLUSIONS

The developed modifications have been successfully implemented and tested in MathCad and Code_Bright. It has been found that the modifications work well and behaves according to what was expected beforehand.

The incorporation of the swelling pressure curve, governing the swelling modulus, gave

the effect wanted; the setting of the parameters does not only become valid for one specific void ratio or a given THM process that must be known prior to the simulation.

The same can be said about the slope of the critical state line; with the modification the parameter set become useful for a broader range of void ratios and THM processes.

APPLICATION OF A DOUBLE STRUCTURE MODEL FOR SWELLING SOILS

Lícia M. da Costa[1], Ivaldo D. S. Pontes Filho[1], Sílvio R. M. Ferreira[1] and Leonardo J. N. Guimarães[1]

[1] Civil Engineering Department
Federal University of Pernambuco
Av. Acadêmico Hélio Ramos, s/n, 50740-530,Recife-PE – Brazil
e-mail: licia@ufpe.br; ivaldo@ufpe.br; srmf@ufpe.br; leonardo@ufpe.br

Key words: expansive soil, double structure model, hydro-mechanical coupled analysis

Abstract. *This paper presents a numerical analysis of the volume change behavior of an expansive soil of the semi-arid region of the northeast of Brazil, due to changes in the water content at different stress level. A coupled hydro-mechanical formulation, implemented in the computational code CODE_BRIGHT was applied to simulate conventional and suction controlled edometric tests performed with this soil. The constitutive model used is the double structure generalized plasticity model proposed by Sanchez et al.(1). Comparison between experimental data and output results of numerical simulations shows a good agreement, checking the capability of the model and the computer code to deal with hydro-mechanical behavior of expansive soils.*

1 INTRODUCTION

In expansive soils, volume change due to applied stress or suction is governed by various phenomena occurring at microstructural level, which means, in individual clay particles and their vicinity. Gens & Alonso(2) presented a conceptual basis for modeling expansive soil, where two different levels are considered: the microstructural level, at which swelling of active minerals takes place and the macrostructural level responsible for major structural rearrangement.

This paper presents an application of a double structure model, proposed by Sanchez et al.(1) and implemented in CODE_BRIGHT to analyze the volume change characteristic, due to changes in water content of expansive soil of the semi-arid region of the northeast of Brazil.

2 NUMERICAL MODEL

The constitutive model adopted in this paper is the double structure generalized plasticity model proposed by Sanchez et al.(1), based on the general framework proposed by Gens & Alonso(2) and considering the improvements suggested by Alonso et al. (3). Two levels of structure are considered. The macrostructure behavior is described by the Barcelona Basic Model (BBM)(4). Other mechanisms, not included in the BBM, which occur in the microstructure, at clay particle level, can take place in expansive soils inducing plastic strains. So the formulation presents the definition of laws for the macrostructural level, the microstructure level and the interaction between both structural levels.

The BBM considers two independent stress variables, the net stress,$(\sigma_{ij}-p_a\delta_{ij})$, and matric suction, $s=(p_a-p_w)$. It is an elastoplastic strain-hardening model, which extends the concept of critical state for saturated soils to unsaturated conditions including a dependence of the yield

surface on matric suction. The yield surface is expressed by:

$$f\left(p,q,s,p_0^*\right) \equiv q^2 - M^2\left(p + p_s\right)\left(p_0 - p\right) = 0 \tag{1}$$

with

$$p = \sigma_m - \max\left(p_a, p_w\right);\ \sigma_m\left(\sigma_1 + \sigma_2 + \sigma_3\right)/3 \tag{2}$$

$$q = \sigma_1 - \sigma_3 \tag{3}$$

$$p_s = ks \tag{4}$$

where p is the net mean stress, σ_1, σ_2 and σ_3 are the total principal stress, M is the slope of the critical state line, p_0 is the apparent unsaturated isotropic preconsolidation stress for suction s, p_0* is the saturated preconsolidation stress, k describes the increase of the apparent cohesion with suction.

For isotropic conditions yield states associated with suction are described by means of a yield function defined in the space (p,s), which is named the Loading-Collapse yield surface (LC). It explains the collapse upon wetting and the increase of apparent preconsolidation stress p_0 with suction through the following relationship

$$\frac{p_0}{p^c} = \left(\frac{p_0^*}{p^c}\right)^{\frac{\lambda(0)-\kappa}{\lambda(s)-\kappa}} \tag{5}$$

with

$$\lambda(s) = \lambda(0)\left[(1-r)exp(-\beta s) + r\right] \tag{6}$$

where κ is the elastic stiffness parameter against changes in p, $\lambda(0)$ is the slope of virgin compression line for saturated isotropic loading, p^c is a reference stress and $\lambda(s)$ is the slope of virgin compression line for isotropic loading at a constant suction s. β controls the rate of stiffness increase with suction and r is a limiting value of soil stiffness for very high suction.

A non associated plastic potential is defined by

$$g\left(p,q,s,p_0^*\right) = \alpha q^2 - M^2\left(p + p_s\right)\left(p_0 - p\right) \tag{7}$$

where α is established in such a way that under K_0 loading lateral strains are zero

The hardening parameters, p_0* depends on the rate of volumetric plastic strain. The hardening law is given by

$$\frac{dp_0^*}{p_0^*} = \frac{(1+e)}{\lambda(0)-\kappa} d\varepsilon^p \tag{8}$$

where e is the void ratio.

Elastic strains are induced by changes in net mean stress, deviatoric stress and suction according to

$$d\varepsilon^e = \frac{\kappa}{(1+e)}\frac{dp}{p} + \frac{1}{3G}dq + \frac{\kappa_s}{(1+e)}\frac{ds}{(s+p_{atm})} \tag{9}$$

The microstructural behaviour is assumed elastic and volumetric. The microstructural volumetric strain depends on a microstructural effective stress ($\hat{p}$) defined by

$$\hat{p} = p + \chi s \tag{10}$$

where χ is a constant

Another assumption adopted in this formulation is the hydraulic equilibrium between microstructure and macrostructure, therefore only one suction variable should be considered.

In the (p,s) plane, a line corresponding to a constant microstructural effective stresses is named neutral line (NL), since no microstructural strain takes place along it. The neutral line divides the (p,s) plane into two parts, defining a compression microstructural stress path and a sweelling microstructural stress path.

The increment of the microstructural elastic strain is expressed as a function of the increment of the microstructural effective stress.

$$\dot{\varepsilon}_{vm} = \frac{\dot{\hat{p}}}{K_m} = \frac{\dot{p}}{K_m} + \chi \frac{\dot{s}}{K_m} \tag{11}$$

where the subscript m refers to the microstructural level, the subscript v refers to the volumetric component and K_m is the microstructural bulk modulus, that in this paper is computed by the following law

$$K_m = \frac{e^{-\alpha_m \hat{p}}}{\beta_m} \tag{12}$$

Microstructural effects induce irreversible macrostructural deformations, which are considered proportional to microstructural strain according to interaction functions.

Two interaction functions are definided: f_c for microstructural compression paths and f_s for microstructural swelling paths. For isotropic loading the interaction functions depend on the ratio p/p_0. In this paper the interaction functions are expressed by

$$f_s = f_{s0} + f_{s1}\left(p/p_0\right)^{n_s} \tag{13}$$

$$f_c = f_{c0} + f_{c1}\left(p/p_0\right)^{n_c} \tag{14}$$

3 APPLICATION OF THE NUMERICAL MODEL

The model described above was implemented in CODE_BRIGHT [(1)], and was used to simulate suction controlled oedometric tests performed with undisturbed soil samples at natural water content of an expansive soil of the semi-arid region of the northeast of Brazil.

The soil presented the following characteristics: w_L = 60%, PI = 30%, w_c = 19%, w = 17.41% and γ_d = 15.05kN/m^3. The initial degree of saturation was 59,24% and suction 5.0 MPa. The parameters used in the simulation are listed in Table 1.

Laboratory data and the numerical simulation results are presented in figure 1. In Test 1, the sample was flooded under a vertical stress of 10kPa and swelling deformation was measured, a volumetric strain of 10% was registered, while in Test 2, inundation occurs under a higher vertical stress (160kPa) the swelling volumetric strain was lower (about 2%).

Parameters defining BBM for macrostructural
$\kappa = 0.009$ $\kappa_s = 0.002$ $\lambda(0) = 0.10$ $r = 0.80$ β (MPa^{-1}) = 10.0 p_0*(MPa) = 0.22 p^c (MPa) = 0.10
Parameters defining the law for microstructural level
χ = 1.0 α_m (MPa^{-1}) = 0.006 β_m (MPa^{-1}) = 0.012
Interaction functions
f_{c0} = -0.10 f_{c1} = 1.5 n_c = 0.50 f_{s0} = -1.50 f_{s1} = 3.70 n_s = 2.0
e_{macro} = 0.80 e_{micro} = 0.30

Table 1: Parameters used in simulation

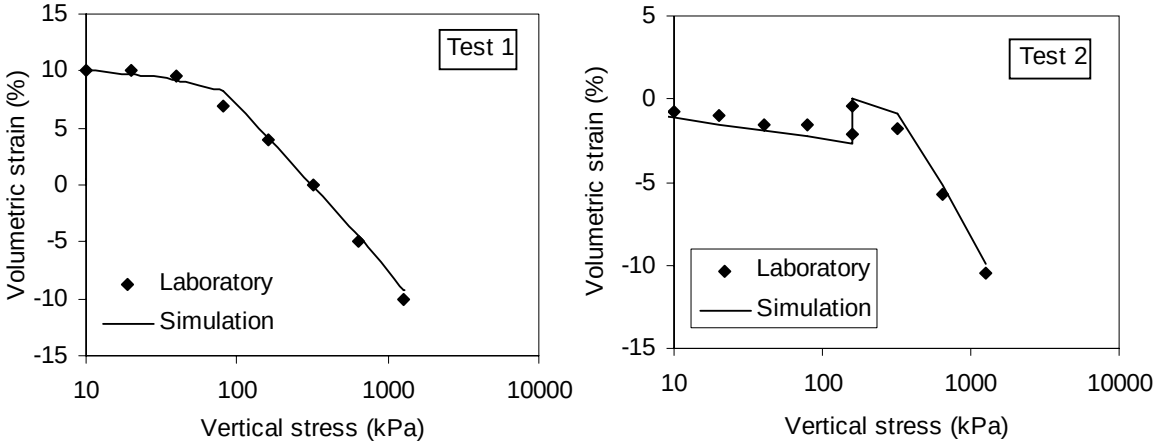

Figure 1: Comparison between laboratory data and simulation results

Comparison between laboratory and simulation results shows a very good agreement with experimental data. Loading under controlled suction and swelling due to suction reduction under a determined vertical stress is very well reproduced for both tests.

4 CONCLUSIONS

The numerical results achieved by the simulation of laboratory tests demonstrate the capability of the model and the computer code to reproduce the hydro-mechanical behavior of expansive soils.

REFERENCES

[1] Sanchez, M., Gens A., Guimarães, L. N. & Olivella, S. 2005. A double structure generalized plasticity model for expansive materials, *Int. J. Numer. Anal. Meth. Geomech.*; vol. 29, pp.751–787.

[2] Gens A., Alonso E. E. 1992. A framework for the behaviour of unsaturated expansive clays. *Canadian Geotechnical Journal*; vol. 29, pp. 1013–1032.

[3] Alonso E, Vaunat J, Gens A. (1999) Modelling the mechanical behaviour of expansive clays. *Engineering Geology*, vol. 54, pp. 173–183.

[4] Alonso, E. E.,Gens, A. & Josa, A. 1990. A constitutive model for partially saturated soils. *Geotechnique*, vol. 40, nº 3, pp. 405-430.

NUMERICAL METHODS IN LABORATORY TESTS DESIGN

Pintado X.[*] and Autio J.[*]

[*] B+TECH Oy, Laulukuja 4, FI-00420, Helsinki, Finland
e-mail: xavier.pintado@btech.fi

Key words: Laboratory, infiltration, thermal test, triaxial test

Abstract. *This paper presents a basis for using model calculations in the design of laboratory tests on bentonite. These calculations find clear application in defining sample dimensions, boundary conditions, and test duration. The calculations are not intended as a substitute for the laboratory tests themselves, but rather are meant to enable the most efficient test design possible.*

1 INTRODUCTION

Compacted bentonite is used as a material to make barriers to prevent contamination isolating the contamination source. High-density compacted bentonite in the form of blocks, discs and rings has also been proposed as sealing material in high-level radioactive waste repositories, as it provides very low permeability, sufficient thermal conductivity and adequate mechanical resistance.

In order to describe the material behaviour, some different models have been proposed. Some thermal, hydraulic and mechanical models are available in CODE_BRIGHT [1] and there is the possibility to couple them, solving different combinations like thermo-hydraulic, hydro-mechanical or thermo-hydro-mechanical problems with different geometries. The mechanical model chosen is the BBM (Barcelona Basic Model, [2]).

It is necessary to know the model parameters to simulate the radioactive waste repository. Laboratory tests are one of the ways to know these parameters because although could be affected by some scale effects, the laboratory allows to control quite good the boundary conditions and the initial states.

The tests simulated in this paper are a water infiltration test, which is used to determine the unsaturated water permeability, a thermal test, which imposes a strong thermal gradient on the sample to in order to determine the tortuosity, a property related to the vapor flow , and a triaxial test.

This work is doing under Posiva's agreement. Posiva is the nuclear waste agency from Finland.

2 DESCRIPTION OF THE TESTS

2.1 Infiltration test

The sample for this test is a cylinder of 50 mm diameter and 70 mm height. The sample is inside a stainless steel cell and it is compacted in this same cell. The test is isothermal with a

constant volume mechanical boundary condition. The hydraulic boundary conditions are defined by a water pressure of 2 MPa on the inlet side and a seepage boundary condition on the outlet side, where the gas pressure is 0.1 MPa.

2.2 Thermal test

This test consists of two samples of 38 mm diameter and 76 mm height separated by a copper heater [3]. The radial strains are expected to be small, so it is run as a thermo-hydraulic case to study the final water distribution and a thermo-hydro-mechanical case to study also the radial strains. The thermal boundary conditions are defined by a constant flux of heat in the copper heater of 2.12 W and constant temperature of 30 °C on the opposite side. The hydraulic boundary condition is zero water flux and the mechanical boundary conditions are given as a vertical strain of -0.135 MPa and a radial strain of -0.101 MPa. Only one of the samples is simulated and the geometry is 3-D with axial symmetry. The finite element mesh has 5 elements in the sample, 10 elements in the thermal insulating bases, 15 elements in the sample height, and 10 elements for the heater height.

2.3 Triaxial test

The triaxial test is simulated with a 3-D mesh. In the triaxial cells, the samples are cylinders, as such σx, σy, σr, and the cell pressure are equivalent. In order to study only those strains far from failure, the 3-D with axial symmetry is sufficient but in failure it is necessary to simulate 3-D geometry because the shearing is not axisymmetric

CODE_BRIGHT does not provide an option for applying pressure to a surface; therefore it is necessary to define all components of the stress. In a cylinder it is necessary to give the components for all nodes manually. This operation takes a lot of time, so it was decided to simulate prismatic samples. The sample simulated is equivalent to a sample of 76 mm height and 38 mm diameter, so its dimensions are 33.66 x 33.66 mm and 76 mm height.

The simulation was performed under isothermal conditions (hydro-mechanical simulation). The gas pressure is constant and equal 0.1 MPa.

The path simulated is as follows:

1. Stabilization of initial conditions with boundary conditions (day 0 to day 1). There aren't any changes.
2. The cell pressure increases from 0.101 to 1.1 MPa (day 1 to day 2).
3. The pore pressure at the bottom increases to 0.9 MPa and at the top to 0.3 MPa, so a gradient is created in order to saturate the sample (day 2 to day 10).
4. This gradient remains from day 10 to day 100.
5. The top pore pressure is increased to 0.9 MPa (day 100 to day 110).
6. The top and the bottom sample remains at 0.9 MPa (day 110 to day 120).
7. The shearing test is performed under constant displacement rate in the axial sense.

3 SIMULATION RESULTS

In order to analyse the influence of the different parameters and boundary conditions in the tests, different simulations have to be done by changing the parameters. This issue is important because it is possible that some parameters do not have any influence on the test and it is not necessary to know them accurately.. One reference case must be chosen to compare the different results. The initial porosity considered was 0.4035 and the initial

suction 133 MPa.

3.1 Infiltration test

The test simulation is hydro-mechanical and the finite element mesh is unidimensional with 100 elements. It is possible to simulate an evaporation rate but then it is necessary to run the problem as thermo-hydro-mechanical.

The main aim of this test is to determine the hydraulic conductivity parameters. In figure 1 the influence of the value of the intrinsic permeability and the relative permeability is displayed.

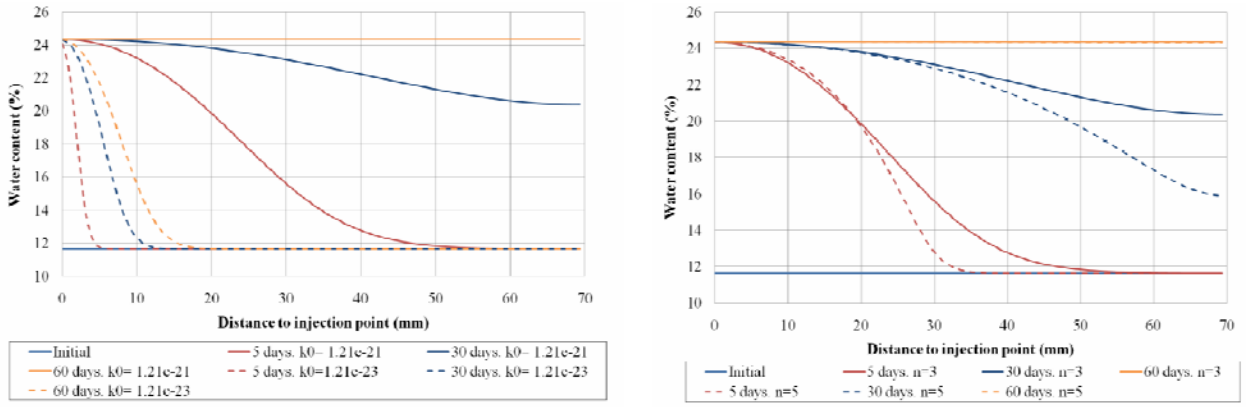

Figure 1: Influence of hydraulic conductivity parameters

3.2 Thermal test

The thermal test allows determination of the parameters related to vapor transport and is able to provide information about the thermal parameters. In figure 2 the temperature and saturation degree distribution after 7 days test are presented.

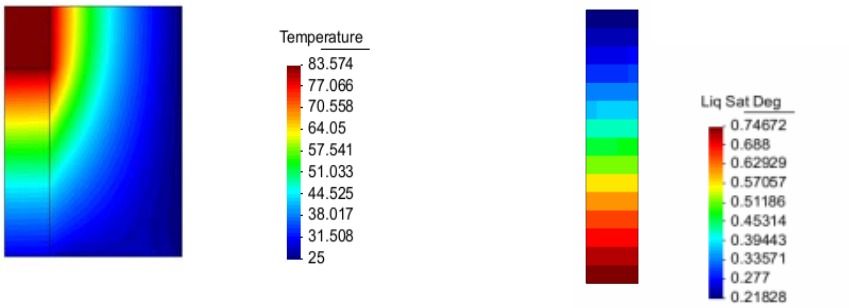

Figure 2: Temperature and saturation degree distribution at 7 days

3.3 Triaxial test

The triaxial test allows analysis of the shear parameters. These parameters are considered constants and don’t change with the saturation degree. It is necessary to reproduce the wetting path to assure the soil structure is similar to the structure of the soil repository, which is

constructed with unsaturated soil and it becomes saturated in contact with groundwater flow. It is important to decide on a reasonable sample size because it takes quite a long time to reach steady state conditions. In figure 3 it is possible to follow the pore pressure evolution inside the sample and the vertical strains in all test steps.

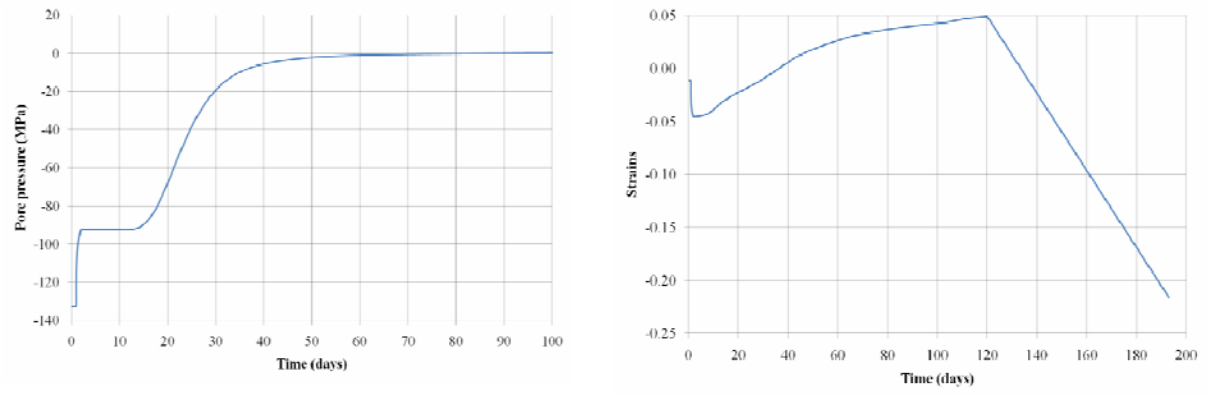

Figure 3: Pore pressure in the central part of the sample and vertical strains in the upper part

The shearing can be reproduced by the test simulation but the numerical process could become unstable. It is out of the scope of this paper to analyze the solution stability near the failure.

4 CONCLUSIONS

- Numerical methods are useful for designing the tests cells and the test plan in order to know the time necessary to do the tests.
- It is necessary to be careful with the unknown boundary conditions. Mistakes in boundary conditions have more severe effects than mistakes in parameters.
- The simulations help to have a better understanding of the phenomena developed during the tests. The processes are quite complicated and the solution is not always intuitive.
- A sensitivity analysis could be useful for the model calibration because the problem has been solved for different parameters.
- The numerical methods give also the possibility to check what parameters are important to explain the sample behavior.

REFERENCES

[1] Olivella, S., J. Carrera, A. Gens, E. E. Alonso, 1994a. Non-isothermal Multiphase Flow of Brine and Gas through Saline media. Transport in Porous Media, 15, 271:293

[2] Alonso, E. E., Gens, A., Josa, A. (1990). A constitutive model for partially saturated soils. Géotechnique 40(3), 405:430

[3] Pintado, X., Ledesma, A., Lloret, A. (2002). Backanalysis of thermohydraulic bentonite properties from laboratory tests. Engineering Geology 64, 91:115

Thermo-hydro-mechanical formulation of joint element and application cases.

María Teresa Zandarín, Sebastián Olivella, Eduardo Alonso.

Department of Geotechnical Engineering and Geosciences
Technical University of Catalonia (UPC)
Campus Norte UPC, 08034 Barcelona, Spain
e-mail: maria.teresa.zandarin@upc.edu; sebastia.olivella@upc.edu; eduardo.alonso@upc.edu

Key words: Joint element, THM coupled analysis, Gas flow interface

Abstract. *In this paper it is presented the results of some examples performed using a thermo-hydro-mechanical formulation of a joint element implemented in Code_Brigth. The numerical simulations involves hydraulic shear tests on joints rock, coupled THM behaviour of interface between canister and expansive bentonite and examples of gas flow trough the interface.*

1 INTRODUCTION

A coupled thermo-hydro-mechanical formulation of the joint element with double nodes is implemented in Code_Brigth [2]. The mechanical problem is formulated by means of the equation of stress equilibrium. The effective stresses are considering applied in the mid-plane and are related with the relative normal and tangential displacements on the mid plane of the element by the mechanical constitutive law [3,5]. The mechanical constitutive law is developed within elasto-viscoplastic framework. The hydraulic problem is achieved by mass balance equation (water and air). The intrinsic permeability and the air entry pressure of the retention curve depend on the interface aperture. The balance of internal energy is established assuming thermal equilibrium between phases.

Three examples have been presented to validate and verify the implementation of the joint element. One of the experimental test simulates are hydraulic shear tests on rough fractures. Other test simulated is a large scale test of a nuclear waste repository (Canister Retrieval Test). And finally it is presented simulations of a made-up case considering gas flow trough interface.

2 HYDRAULIC SHEAR TEST ON ROUGH FRACTURES

The hydraulic shear tests were performed by Lee, et al [4] in rock joints of granite from Korea. The main objective of the tests was to measure the permeability of the joints during a shear tests. The tests were carried out maintain constant the normal stresses of 1, 2 and 3 MPa. The tangential displacement was applied with a rate of 5mm/seg. The hydraulic pressure applied on the joint varied from 4.91 kPa to 19.64 kPa. For each stage of shear displacement of about 1mm, the hydraulic pressure was kept constant. When the fluid flow reached steady state, mean flow rate was calculated based on the amount of outflow measured for the period of 2 minutes. And these measures were used to calculate the permeability of the joint.

The results obtained from the simulation are comparing with tests results in Figure 1 a, b and c. The mechanical behaviour of the joint is closely reproduced by the model. The numerical formulation is able to reproduce the increment of peak shear stress with the normal

stresses. Also, it is possible captured the decrease the shear strength with displacements. Moreover, the dilatancy of the joint is also captured (Figure 1 b).

The evolution of the intrinsic permeability of the joints is also simulates. Even thought, permeabilities of the model increase continuously, the permeability of the tests for different normal became almost the same. This is mainly caused by the gouge materials generated from the degradation of asperity during shearing; which it is not considered in the model (Figure 1 c).

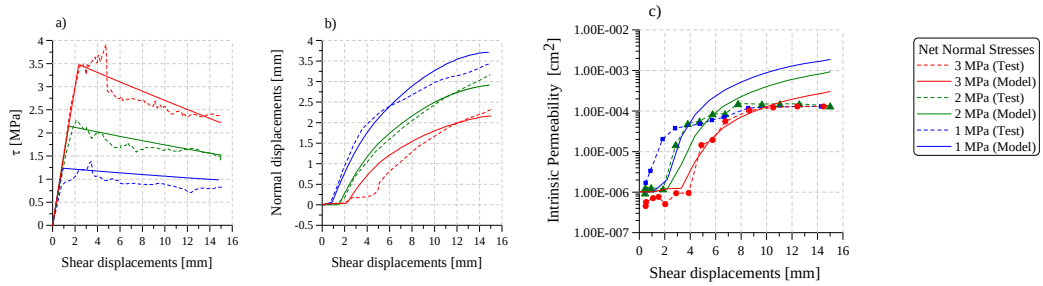

Figure 1: Comparison between experimental results obtained by Lee et al.(2002)[4], and results from numerical simulation. a) Shear stress-shear displacements curve. b) Normal displacements vs. shear displacements and c) Intrinsic permeability vs. shear displacements.

3 LARGE SCALE TEST OF NUCLEAR WASTE REPOSITORY (Canister Retrieval Test)

A thermo-hydro-mechanical simulation of Canister Retrieval Test (CRT) [1] was performed modelling the interface between canister and bentonite as a joint element (Figure 2 a). In Figure 2 b and c it is shown that the mechanical behaviour of the joint element (evolution of its opening and its horizontal stress) depends on the swelling or contraction of the bentonite [6].

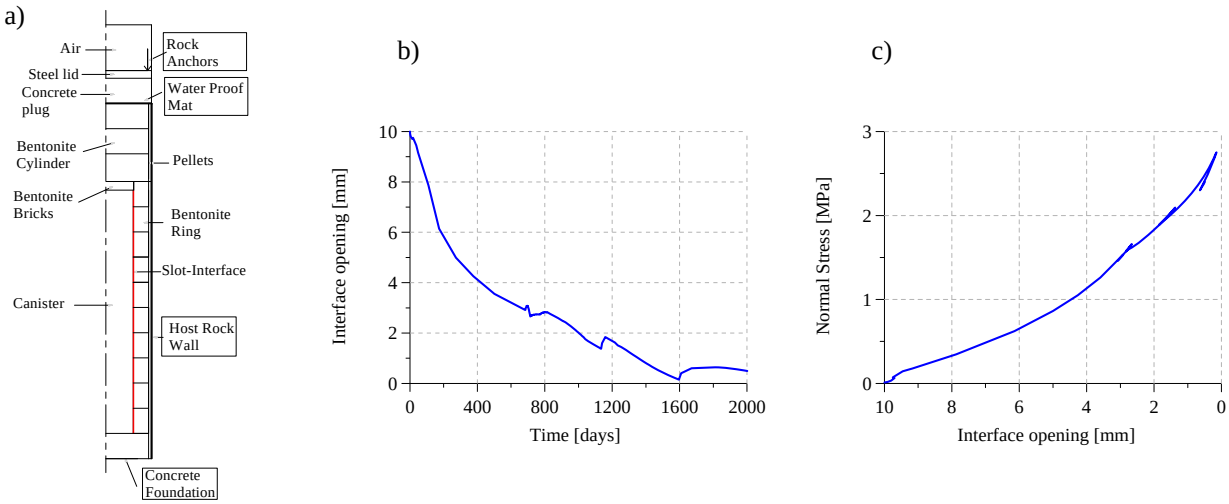

Figure Nº 2 Large scale test Canister Retrieval Test. a) Geometry of the model simulated. b) Evolution of the interface opening. c) Evolution of the horizontal stress of the interface.

4 STUDY OF THE GAS FLOW TROUGH CANISTER-BENTONITE INTERFACE

This study was performed with the objective of evaluate the behaviour of the interface element subjected to a thermo-hydro-mechanical conditions and gas flow. The motivation of

performed these examples is the fact that gas generation take place in radioactive waste repositories due to the corrosion of canister.

Even though the examples model it is very simple because only one point on the middle depth of canister is considered as a gas flow source. These examples allow perform some calculation to evaluate the gas pressure generation and the gas fluxes regarded different interface and bentonite properties. The examples calculated considers changes of gas permeability of bentonite, changes on interface capillary pressure and changes of mechanical properties of interface and its implication on gas flow. The gas flow rate injected is 10^{-7} kg/s and it is injected after a hydration phase which takes 2000 days. The gas injection also extends 2000days.

For instance in Figure 3, 4 and 5 it is shown the results obtained for Case 1. In this case the initial gas permeability of the bentonite is kg = $2.62x10^{-14}$. And in Figures 6, 7 and 8 it is shown the results obtained when the initial gas permeability of the bentonite adopted is kg = $2.62x10^{-16}$ (Case 2).

For Case 1 the gas pressure is lower than Case 2 and only affects the zone closer to the injection point (see Figure 3a and 6a). Then, the interface opens by the increment of the gas pressure when it is injected. After part of the gas injected begins to flow trough the bentonite, and the interface begins to close again due to the swelling of bentonite (Figure 4). This implies that permeability decrease and air pressure entry increase and as consequence the degree of saturation of interface increase during the injection of the gas (Figure 5).

In Case 2 as bentonite has a lower permeability the gas flow along the interface, this cause that gas pressure is higher than in Case 1 and its affect the total length of the interface and bentonite (Figure 6). This implies that interface aperture be higher that in Case 1 and this increment extend along interface length. A consequence of this it is a sudden increment of interface permeability and a sudden decrease of the air entry pressure (Figure 7). This involves a great decrease of the degree of saturation of the interface and little rate of its hydration after the start of the injection.

Then, in Case 1 only a zone close to the injection point desaturate in coincidence with the zone where the gas pressure increase. But in Case 2 the desaturation extend along the length of the interface. However, the bentonite desaturation extends up to a radial distance equal 550mm in both cases.

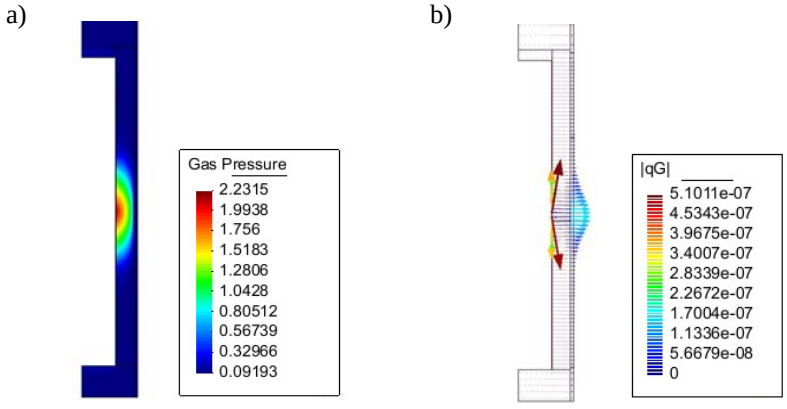

Figure 3 a) Gas pressure at day 4000, b) gas flow at day 4000. Case 1

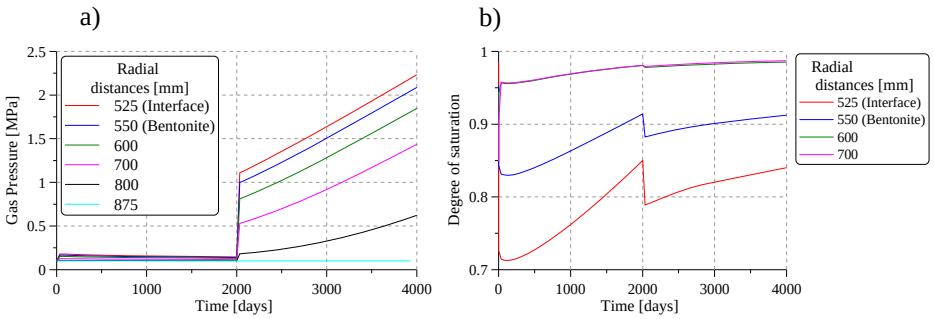

Figure 4 a) Evolution of gas pressure at interface and bentonite buffer for different radial distances. b) Evolution of degree of saturation for the interface and bentonite buffer. Case 1

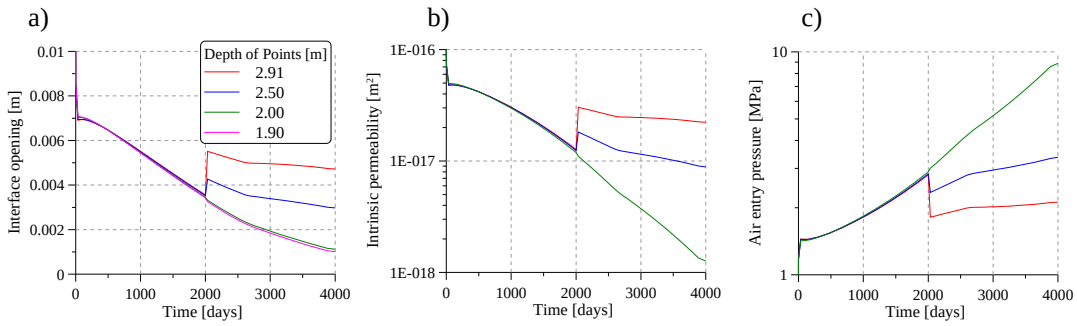

Figure 5 a) Evolution of interface opening before and after gas injection. b) Evolution of interface permeability and c) Evolution of air pressure entry. Case 1.

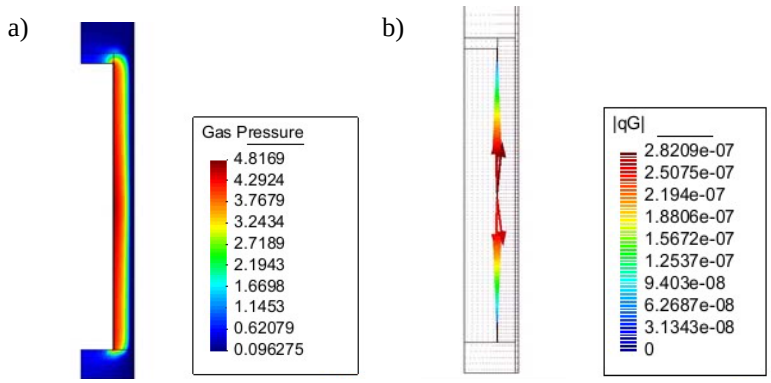

Figure 6 a) Gas pressure at day 4000, b) gas flow at day 4000. Case 2

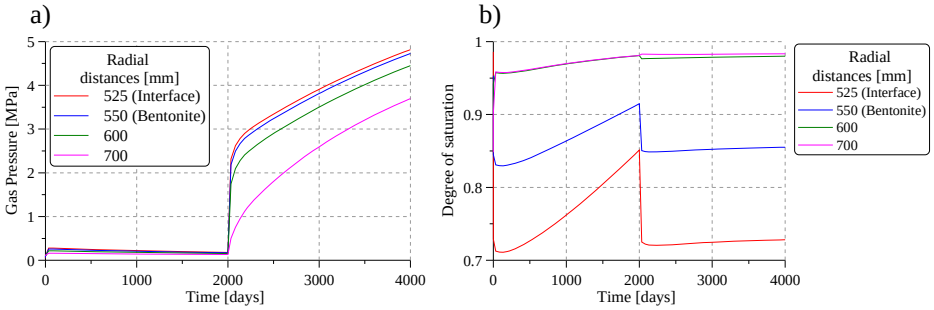

Figure 7 a) Evolution of gas pressure at interface and bentonite buffer for different radial distances. b) Evolution of degree of saturation for the interface and bentonite buffer. Case 2

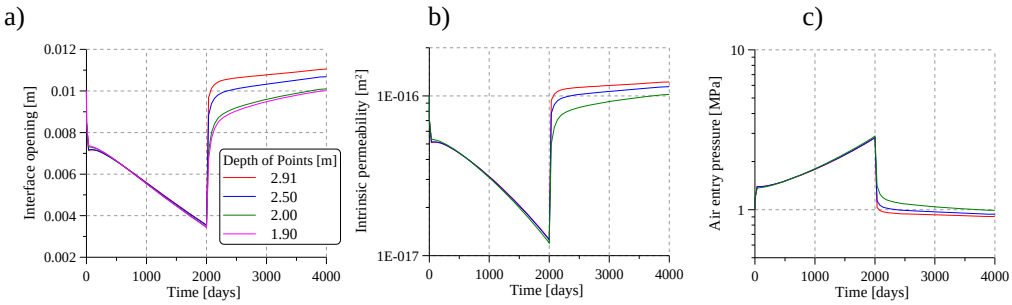

Figure 8 Evolution of interface opening before and after gas injection. Case 2.

4 CONCLUSIONS

- A thermo-hydro-mechanical joint element has been implemented into Code_Bright.
- Comparing the experimental data obtained by Lee, et al. and the numerical results is concluding that the joint formulation is capable to reproduce the main characteristic of the coupled joint behavior. For instance, it is well captured the shear stress softening and dilatancy with shear displacements as the increments of permeabilities with displacements.
- The results obtained from the simulation of the CRT it was possible to verify that the model implemented for interfaces is able to capture the THM interface behaviour. And it is shown that the evolution of its opening and stress depends mainly on the bentonite swelling.
- And finally from the results obtained from the numerical simulation considering a gas rate injection it was possible analyze the gas flow trough the interface changing the gas permeability of the bentonite. And also study the influence of the changes of hydraulic properties of the interface due to the evolution of its aperture.

REFERENCES

[1] Börgesson L., 2007. Canister Retrieval Test, Compilation made for the EBS Task Force.

[2] DIT-UPC. 2000.CODE_BRIGHT. A 3-D program for thermo-hydro-mechanical analysis in geological media. User's guide. Barcelona: Centro Internacional de Métodos Numéricos en Ingeniería (CIMNE).

[3] Gens, I. Carol, and E.E. Alonso 1990. A constitutive model for rock joints; formulation and numerical implementation. Computers and Geotechnics, 9:3–20,.

[4] Lee, H.S. and Cho, T.F. 2002.Hydraulic Characteristics of Rough Fractures in Linear Flow under Normal and Shear Load. Rock Mechanics and Rock Engineering,35(4),229-318.

[5] Segura J. Ma. 2008. Coupled HM analysis using zero-thickness interface elements with double nodes. Tesis de Doctorado-Universidad Politécnica de Catalunya, Barcelona.

[6] Zandarín M.T., Olivella S., Gens A., Alonso, E.E. (2010) "Thermo-Hydro-Mechanical Model of Canister Retrieval Test." 4th International Meeting on Clays in Natural & Engineered Barriers for Radioactive Waste Confinement, Nantes. (Accepted)

NUMERICAL SIMULATIONS FOR SOIL-ATMOSPHERE INTERACTION ANALYSIS

Marco Caruso*

*Structural Engineering Department
Politecnico di Milano
Piazza Leonardo da Vinci 32, 20133 Milano, Italy
e-mail: caruso@stru.polimi.it, web page: http://www.stru.polimi.it

Key words: soil-atmosphere interaction, hydrologic balance, boundary conditions, soil-atmosphere fluxes

Abstract: *A series of numerical simulations, preceded by sensitivity analysis have been proposed in a research program confirming the capabilities of CODE_BRGHT to be a suitable tool for the analysis of a soil atmosphere interaction problem. Numerical results can easily allow to obtain water fluxes (both liquid and vapour) exchanged at the ground level and water mass stored into a reference soil volume. However to obtain reliable results, some attention has to be paid to time discretization for boundary condition and for post-processing of boundary flux data.*

1 INTRODUCTION

Soil water content dynamics in the soil layers closest to the atmosphere interface play a key role in many environmental applications. As an example they can influence shallow water-table fluctuations and groundwater reservoir recharge and discharge (Wu & Zang[i], Gowing et al.[ii]) and at the hillslope scale, soil moisture distribution is a controlling factor in the hydrological and mechanical processes responsible for slope instability and shallow landsliding.

There is a wide-accepted evidence that the distribution and movement of water in the unsaturated zone near earth surface is strongly affected by the interaction with the atmosphere (Milly[iii]). A summarized way to describe the response of a soil volume to environmental loading is be *soil water balance*, which sum up the effects of the unsaturated (or saturated) flow through the considered portion of soil and the water mass exchanges between soil and atmosphere.

Since nowadays experimental techniques allow to obtain local (almost punctual) information without incurring in high costs, the numerical approach appear to be the only capable to give soil water balance estimation over large areas and long periods and, of course, its prediction for definition of future scenarios. Given that, CODE_BRIGHT (Olivella et al.[iv]) has been employed to estimate the soil-water balance over an extended area (Caruso[v]), by calibrating the parameters from a dedicate laboratory and in-situ experimental program. The development of the numerical model was preceded by a series of short-period sensitivity analysis (reported in detail by Caruso[v] and Caruso & Jommi[vi]) devoted to the comprehension of the different modelling choices impact, after which a long period simulation has been carried out, obtaining encouraging result both in direction of model validation and of its prediction capabilities.

2 NUMERICAL MODEL

Giving an almost flat and homogeneous study area, as well as for meteorological conditions, following Milly[iii] suggestions, the recommended reference approach could be 1-dimensional, in which the water exchanges between soil and atmosphere (both in vapour and in liquid phase) are possible at the ground level. Its implementation in CODE_BRIGHT, given the way the boundary condition and initial condition can be assigned, has lead to the adoption of a 2D very thin vertical soil column (0.002 m large). The two-dimensional approach in fact, despite of doubling the total number of nodes (reaching a total of 482 nodes with 240 elements for the set of simulation presented here), is the only allows to assign the element porosity and that gives the possibility, adopting the adequate index, to reproduce in the correct way the desired conditions at the soil atmosphere interface: uniformly distributed along the boundary and, in case of a flux-type one, directed inward or outward from the soil ad normal to the soil ground level.

All the remaining column boundaries (right, left and bottom) are supposed to be perfectly watertight and the entire soil column is considered homogeneous. The mesh adopted is a structured one (quadratic) with an element concentration at the top since higher gradients have to be expected. The smallest element has about 1 mm high.

A two months real sequence of rainy and evaporation events (in terms of rain intensity, temperature, relative humidity, solar radiation and wind velocity), was simulated, starting from an initial condition of soil near to saturation (recorded from an experimental monitoring program).

3 NUMERICAL RESULTS

The different numerical simulations proposed had the major goal to evaluate the consequences of the different numerical choices. Among the others a first set of analysis has been proposed to deal with the possibility to use a one phase approach, just by solving the mass balance of water and translating the atmospheric boundary conditions in a constant inflow rate combined with a run-off condition ($\gamma_l < 0$) for rainy intervals, while imposing a non rainy condition in terms of pore water pressure, supposed to be in equilibrium with the atmosphere following the psychometric law. The alternative way is to solve a 2 phase (liquid and gas) and temperature fully coupled problem. Redirecting to literature for a discussion of the opportunity to analyze the problem in a fully coupled way, here numerical result from both approaches are presented to analyze the points to which attention must be paid in boundary conditions imposition and in result post-processing.

3.1 Boundary condition

The boundary conditions were discretized hourly, thanks to meteorological information availability for the study case. The possibility of imposing daily boundary condition has been evaluated, being a way to reduce time steps to be processed and, if necessary, to employ daily recorded meteorological data. The reference two-month interval has been divided into non rainy and rainy day: the rainy days precipitation is uniformly distributed over 24 hours, while the mean value for temperature, air pressure, relative humidity, wind velocity, etc. are considered for non rainy days. Result are reported in figure 9 in terms of degree of saturation changes over the time at two different depth. The outstanding role of time scale can be pointed out, since it’s immediate to notice how the daily discretization leads to an higher infiltration of water inward upper soil layers. The degree of saturation obtained with a daily

analysis is always higher than the corresponding one coming from the hourly information. With the day approach, in fact, it's not possible to take into account the important run-off effect associated with high intensity and short duration rainy events.

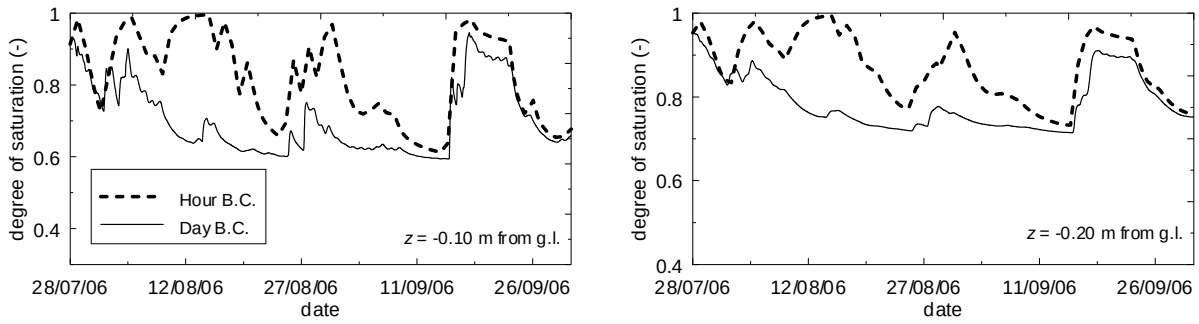

Figure 1. Comparison between hourly and daily b. c. for a coupled two-phase and temperature analysis

3.1 Water balance

The results of each simulation (degree of saturation, phase pressure and densities, and, when applicable, mass fraction of species in different phases, boundary fluxes) can be the basis for the evaluation of the water balance over the simulated interval. The balance can be expressed, among others, in terms of water mass flux exchanged at soil atmosphere interface and in terms of total water mass exchanged over a desired interval. The total water mass is intended as the sum of liquid and vapour water mass.

The exchanged fluxes or the cumulated mass may be obtained in two different ways, both implemented in a set of developed post-processing tools. The first one directly takes the information provided by analysis output for boundary fluxes which are subsequently integrated for cumulate masses. In this way liquid and vapour fluxes at boundary can be identified obtaining the amount of water exchanged as their sum. The second one is based on the evaluation of the total water mass (both in liquid and vapour phase) stored into soil column. Its time variation describes the cumulated information from which instantaneous fluxes can be derived. This "stored water mass" procedure is suitable to give information only about total mass, and it does not allow to identify the liquid and vapour components.

Different tests seem to suggest that the second approach should be preferred since the first one may lead to some error. A comparison between the fluxes exchanged in a one-phase liquid simulation from stored water mass evaluation and from boundary flux output values is presented in figure 2. Observing a significant overestimation of total exchanged mass in the boundary flux approach a new analysis has been carried out, allowing the code to write all output information neglecting the large increase in total solving time and disk occupation.. This means now boundary flux are stored for every calculation time step instead of the previous simulation, for which output information were written about every hour. The new mass exchange estimation now seems to be closer with the one obtained from stored mass. It is important to notice that all flux values are hundred times the mass information values.

A possible explanation to the observed issue has been attributed to the way in which the boundary condition are imposed and the boundary fluxes are written out. It seems that, due to the multiplier approach for boundary condition (CODE_BRIGHT manual), when time step become small (also of magnitude order of 10^{-7} s, necessary for numerical convergence) the flux rate become very high (figure 3). This happens mostly when boundary condition are

changed. Even if very high, the flux gives an almost null contribution to the amount of total water exchanged due to its short duration. On the other side, the code gives the option to write boundary fluxes with a user-define frequency, which is based only on number of processed time steps. If the time step chosen for writing output information is the one in which the peak is reached, the post-processing integration in time for cumulate mass estimation will be significantly affected since an high flow rate is erroneously supposed.

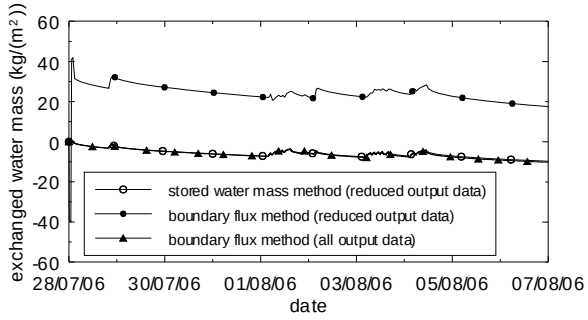

Figure 2. Cumulated water mass at soil atmosphere estimated from different methods

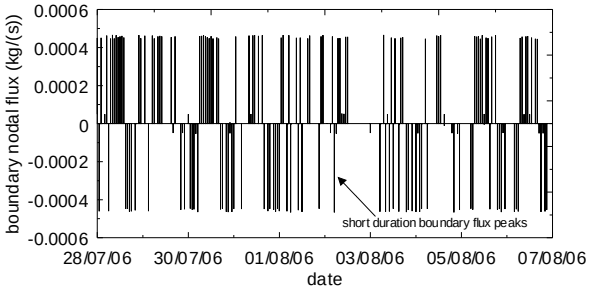

Figure 3. Boundary flux sequence as in output files

4 FINAL REMARKS

A series of numerical simulation and developed post-processing tools have confirmed the possibility to obtain reliable information on hydrologic balance using CODE_BRIGHT. In this context it is worth pointing out that the choice of the time interval for boundary condition discretization may have an influence on predicted response of soil in terms of water distribution (and in terms of water balance). Moreover, the reduction of the output writing frequency appear to be possible for the major part of the output data without loosing the capability to reproduce mass water exchanges history at soil atmosphere interface. Conversely, it appear that water balance can be obtained from boundary flux without incurring in overestimation if output information are registered for all calculation time steps.

REFERENCES

[i] Wu J., Zhang R., 1994. Analysis of rainfall-infiltration recharge to groundwater. In H. J. Morel Seytoux (eds), *Proc. of 14th annual american geophysical union hydrology days. 5-8 April 1994, Fort Collins, Colorado*: 420-429

[ii] Gowing J.W., Konukcu F., Rose D. A. 2006. Evaporative flux from a shallow watertable: the influence of a vapour-liquid phase transition. *J. of Hydrology* 321(1-4): 77-89

[iii] Milly P. C. D. 1988. Advances in modeling of water in unsaturated zone. *Transp. in por. media* 3: 491-514.

[iv] Olivella S., Gens. A, Carrera J., Alonso E. E., 1996. Numerical formulation for a simulator (CODE_BRIGHT) for the coupled analysis of saline media. *Eng. comp*. 13: 7–112.

[v] Caruso M., 2007. Una metodologia teorica, sperimentale e numerica per la previsione del bilancio idrico nei terreni superficiali non saturi. Ph. D. thesis. University of Parma, Italy

[vi] Caruso M., Jommi C. (in press). Numerical modelling of near surface soil water content changes over a long time period. Proc. of 3rd IWUS08 - "Between Theory and Practice in Unsaturated Soil Mechanics". Trento 4th-6th February.

MULTIPHYSIC SOIL - PLANT - ATMOSPHERE INTERACTIONS USING FINITE ELEMENT CODE - CODE_BRIGHT

S. Samat[1], J. Vaunat[1], M.W. Saaltink[1], J.-M. Pereira[2], E. Martin[3], J. Darrozes[4] & D. Virely[5]

[1] Department of Geotechnical Engineering and Geosciences, Technical University of Catalonia (UPC), Barcelona, Spain
[2] Laboratoire Navier École des Ponts ParisTech, Université Paris-Est, Marne-la-Vallée, France
[3] CNRM-GAME, Météo-France, Toulouse, France
[4] Laboratoire des mécanismes et transferts en géologie, CNRS, Toulouse, France
[5] Laboratoire Régional des Ponts et Chaussées, Toulouse, France

Key words: Radiation, Precipitation, Evapotranspiration, aerodynamic resistance, surface stomatal resistance, sensible heat, latent heat.

Abstract. *The abstraction of soil water by vegetation and its influence on the behavior of geotechnical structures such as pavements, foundations and slopes has been researched for many years. A major challenge for numerical modelers, in geotechnical engineering, involves the specification of the surface flow boundary condition to model root water uptake by vegetation. The abstraction of soil water by roots is a complex process which involves the interaction of the atmosphere, vegetation and the soil. Accurate prediction of the pore water pressure changes induced by vegetation requires the development of algorithms which can reproduce the process of transpiration by vegetation in the continuity equation of fluid flow. This paper presents a model of heat and mass exchanges at the land surface to be used in soil-atmosphere interaction models. The vegetation with its canopy interacts both with the soil-surface and the atmosphere. The model calculates abstraction of soil water by vegetation (transpiration) using atmospheric data (atmospheric temperature, radiation, relative humidity, wind velocity) as a function of the soil's state variables:* (T)*, temperature,* (p_l)*, liquid pressure and* (p_g)*, gas pressure; taking into account aerodynamic and stomatal surface resistance. Likewise it calculates evaporation and heat exchange between the soil and atmosphere. The soil-plant-atmosphere model was implemented in the multiphysics "Thermo-hydro-mechanical" coupled finite element code CODE_BRIGHT. The key features of the model are discussed by means of a series of parametric studies.*

1 INTRODUCTION

The water uptake due to plant transpiration is probably the main issue of Soil-Vegetation-Atmosphere transfer schemes because of its major influence on soil moisture. The influence of vegetation on pore water pressures and ground movements involves the interfacing of dynamic factors of the atmosphere, vegetation and soil. To quantify both, the water loss due to transpiration and the volume change in the ground, the development of water uptake models which can reproduce transpiration are necessary. This transpiration flux, from the rooting system, depends on vegetation physiology: *LAI*, leaf area index; *veg*, canopy index; R_s, surface stomatal resistance. The last one is largely driven by environmental conditions and soil moisture availability, being enhanced in conditions of full radiation, moderate atmospheric

specific humidity deficit, optimum air temperature and freely available soil water in the rooting zone. In contrast to models in which root water uptake is only a function of the pore water pressures within the ground, the present provides more realistic fluxes of sensible heat, latent heat, water and energy, interchanging between the soil-atmosphere interfaces. Once presented the development of the mathematical soil-vegetation-atmosphere model, the numerical results are shown due to atmospheric loads applied over a soil column. The evolutions of volumetric water soil content and temperature are of important consideration. Three different meshes were tested, in order to study its effects in computing the transpiration flux. Finally some conclusions are given in terms of the previous results.

2 MATHEMATICAL MODEL

The water uptake flux at different depths below the ground surface becomes governed by the root density, conductivity of soil root system and the availability of soil water. In numerical analysis the transpiration flux is taken into account by incorporating a sink term of water mass. Based on J.Noilan and S.Planton [1989], the following formula is propose

$$E_v = veg \cdot \frac{1}{R_s + R_a} \cdot (\rho_{va} - \rho_v) \qquad (1)$$

Where R_s and R_a are the surface stomatal resistance and the aerodynamic resistance respectively and act as resistances to the water extraction from plant's root system; ρ_{va} is the absolute humidity of the atmosphere and ρ_v is the absolute humidity at the node of the plant's root, respectively. Both can be calculated from the relative humidity and temperature. The difference (ρ_{va}- ρ_v) acts as a potential of the soil-root-atmosphere system (fig1). The expression for the surface resistance R_s depends on both atmospheric factors and available water in the soil, it is given by

$$R_s = \frac{R_{s_{min}} \left(1 + \frac{1.1}{LAI} \cdot \left(\frac{R_g}{R_{g_1}}\right)\right)}{1.1 \left(\frac{R_g}{R_{g_1}}\right) + \beta \cdot LAI} \cdot F_2^{-1}(\theta) \cdot F_3^{-1}(p_{v_{at}}) \cdot F_4^{-1}(T_{at}) \qquad (2)$$

Where the first term of the product in the right hand side measure the influence of the photosynthetically active radiation. The factor F2 describes availability of water in the root

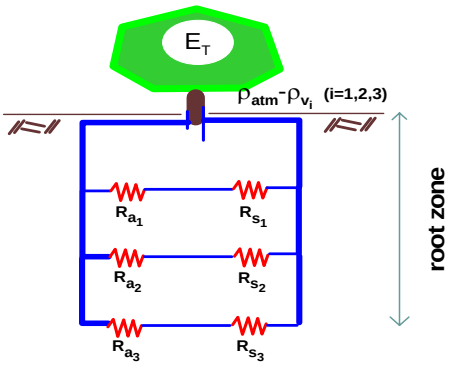

Figure 1: Soil-Root-Atmosphere assumed model

zone for transpiration; it varies between 0 and 1. The factor F3 represents the effects of vapor pressure deficit of the atmosphere, demonstrated by Jarvis [1986]. The factor F4 introduces an air temperature dependence on the surface resistance, Dickinson [1984].

3 NUMERICAL SIMULATIONS

The numerical simulations were performed on a one dimensional soil column. The initial conditions assumed a hydrostatic pore water liquid of 0.8MPa at the top and 0.27MPa at the base of the mesh, a constant gas pressure 0.1MPa was assumed, implying that the phreatic surface is located at 2 meters depths. Linear elastic material properties were assumed for the soil with a Young's modulus of 30MPa and a Poisson's ratio of 0.3. The specific heat of the solid matrix was taken as $800Jk_g^{-1}K^{-1}$, while the solid density as $2700kgm^{-3}$. The soil was assumed to have a uniform permeability of 2.6e-8 m/s. The analyses were carried out with a 1m maximum root depth. Three different mesh configurations were selected, identify by, the ratios of element thickness to maximum root depth and the density of elements below the root zone: 0.25+fine mesh (vfmesh), 0.125+fine mesh (vgmesh) and 0.25+ thick meshes (vpmesh). Figure (2) shows the sensitivity of Evapotranspiration model through, temperature and pore water pressure variations with depth for the mentioned meshes.

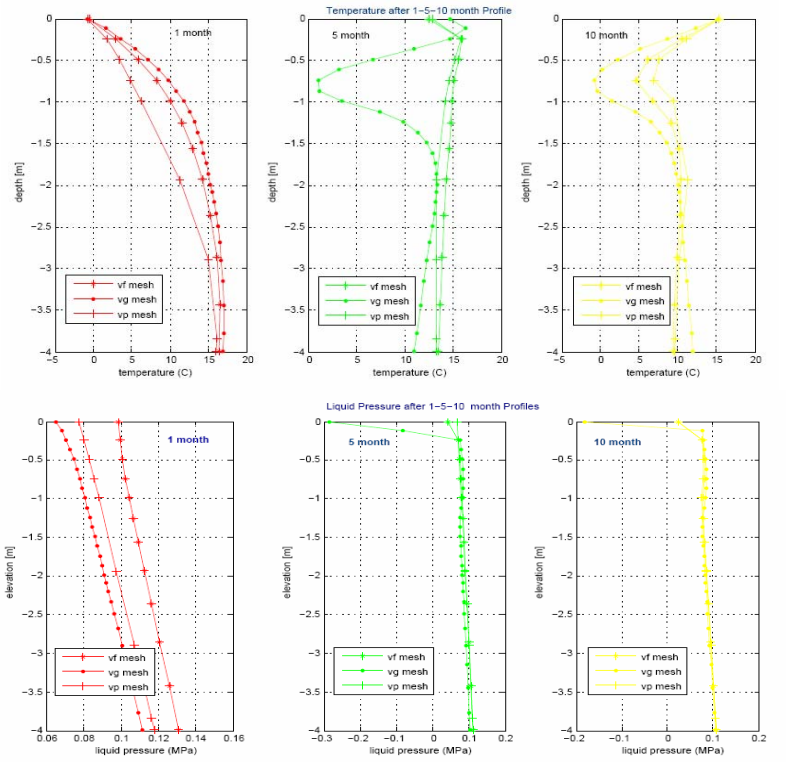

Figure 2 : Temperature and Pore Water Pressure variations with depth for different mesh configurations

The atmospheric data used in the simulations to known; Temperature (T), Gas Pressure (Pa), Relative Humidity (Hr), Radiation (Rn), Cloud index (In), Rain (P), Wind (va); was measured by Meteo-France Department at Le Fauga site. Figure (3) shows the evolutions of water content and temperature at three different depths. They exhibit a very good agreement with respect to the measured data.

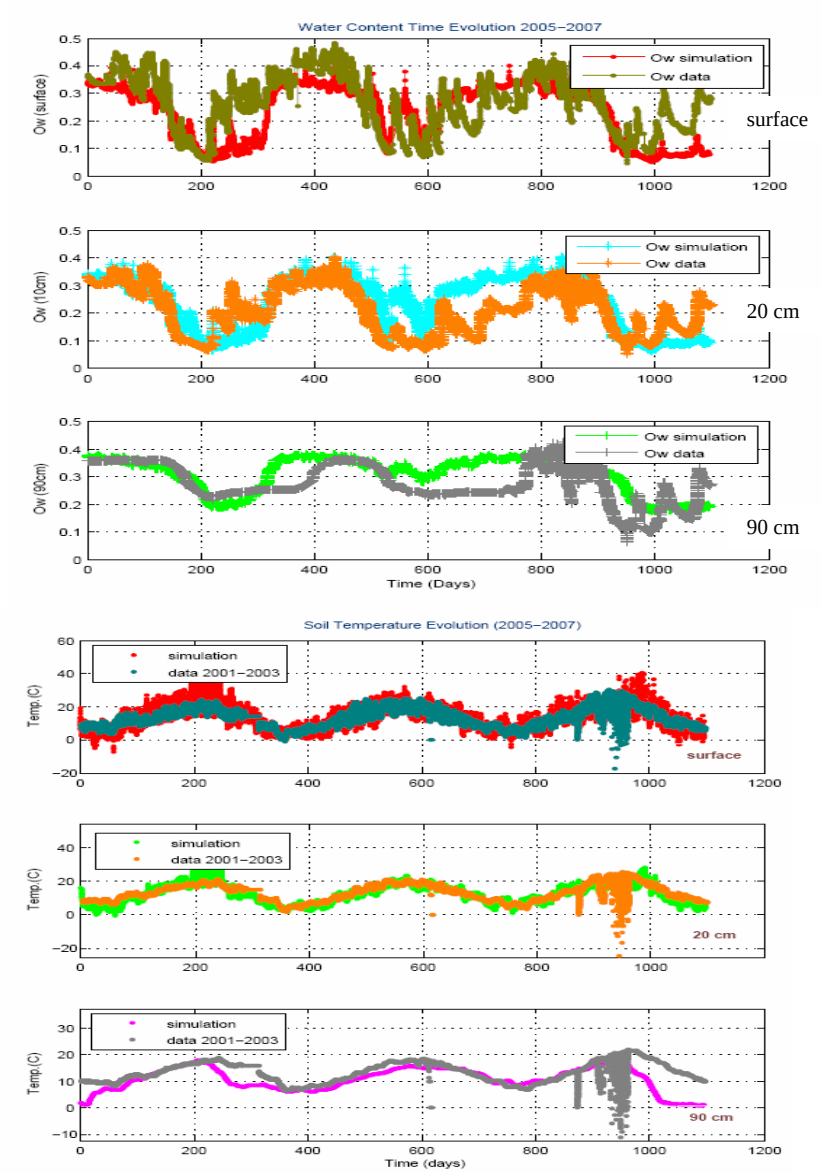

Figure 3: Computed *vs* measured evolutions of volumetric water content and temperature (period 2005-2007)

ACKNOWLEDGEMENT

The authors acknowledge Meteo-France for providing the meteorological data at Le Fauga site and the support of the European Commission through the FEDER grant SOE1/P2/F57.

REFERENCES

[1] J.Noilan and S.Planton, 1989. A Simple Parameterization of Land Surface Processes for Meteorological Models. Monthly Weather Review, vol. 117, pp. 536-549.

MODELLING TWO PHASE FLOW IN STRESS SENSITIVE PETROLEUM RESERVOIR

Igor F. Gomes[1], Leonardo J. N. Guimarães[2] and Lícia M. da Costa[1]

[1] Department of Technology
Academic Center of Agreste – Federal University of Pernambuco
Rodovia BR 104, Km 59, s/n, 55002-970, Caruaru-PE, Brazil
e-mail: gomes@ufpe.br; licia@ufpe.br

[2] Civil Engineering Department
Federal University of Pernambuco
Av Acadêmico Helio Ramos, s/n, 50740-530, Recife-PE, Brazil
Email: leonardo@ufpe.br

Key words: two phase flow, geomechanics, hydro-mechanical coupled analysis

Abstract. *This paper presents a formulation implemented in CODE_BRIGHT to simulate fluids flow in petroleum reservoir sensitive to stress state. In this program the equations of two-phase flow problem are solved together with the stress equilibrium equation, which characterize the geomechanical problem. One example of application is presented where two-phase flow in the reservoir is simulated considering three different situations; in the first one the reservoir is considered a rigid medium, while in the two other analyses the reservoir is considered a deformable medium. Comparisons among the analyses carried out show the influence of geomechanical coupling in oil recovery during primary production stage.*

1 INTRODUCTION

Changes in pore pressure, temperature and water saturation in hydrocarbon reservoir occur due to depletion or injection processes[i]. This lead the reservoir and adjacent rocks to stress state changes (reduction of the effective stress due to pore pressure increase), which can generate rocks deformation processes, as compaction and subsidence phenomena, that change their properties (solid matrix) and, in some cases, cause problems such as fractures development, faults activation and wells damage. On the other hand, the compaction phenomenon can also improve hydrocarbons production, delaying pore pressures reduction during exploitation.

In fact, the coupled flow problem in deformable porous media[i] [ii], i.e., the interaction between the geomechanical response and fluids behavior, has being widely discussed in numerical studies of hydrocarbon production process in petroleum reservoir[iii]. The flow equations are modified by incorporating rock deformation, while the mechanic equations will include a pressure and saturation term from the flow equations.

In this paper it is discussed the reservoir compaction problem and its effect in the primary fluid production. Thus two phase (water and oil) flow problem, which unknowns are the water saturation (S_w) and oil pressure (p_o), is solved together with the stress equilibrium equation, for the geomechanical problem, which unknowns are rock displacements (u). The numerical scheme for the solution of the two phase flow problem considered in this paper is the Sequential Implicit Method[iv], where the geomechanical problem is solved sequentially to the

two phase problem, and the unknowns are updated simultaneously to each Newton-Raphson interaction in both problems. This method (sequentially implicit) proved to be very efficient when applied in high coupling levels problems, such as reservoir compaction.

2 MATHEMATICAL FORMULATION

In the two phase (water and oil) flow model used in this paper, the equation which governs the problem is:

$$\frac{\partial(\phi S_\alpha \rho_\alpha)}{\partial t} + \nabla(\rho_\alpha q_\alpha + \phi S_\alpha \rho_\alpha \dot{u}) = 0 \qquad \alpha = w, o \tag{1}$$

where S_α and ρ_α are the phases saturation and density, respectively. The subscript α represents the phase, that can be *w* for water phase or *o* for oil phase, ϕ is the rock porosity, $\dot{u}$ represents the rate of displacement of the solid phase and q_α is the fluid flow with respect to the solid phase (Darcy's Law).

The mechanical problem is governed by stress equilibrium equation that is defined by the sum of the divergent of total stress σ added to body forces vector b, as follow:

$$\nabla \boldsymbol{\sigma} + \mathbf{b} = 0 \tag{2}$$

Applying Terzaghi's Effective Stress Principle, the total stress is related with the effective stress σ' and pore-pressure p_s according to equation (3):

$$\sigma = \sigma' + S_o p_o + S_w p_w \tag{3}$$

where the pore pressure is defined as function of phases pressures p_α and saturations S_α.

For the elastoplastic analyses this paper uses the Modified Cam-Clay mechanical constitutive model[iv] [v], that is interesting to reproduce the reservoir compaction phenomena. The compression state is generated inside the reservoir due to the increase of the effective stress caused by pore-fluid reduction, after production wells opening. The porosity and permeability properties of the porous media work as coupling variables between the geomechanical module and flow equations, where both are updated to the new effective stress state and so to the material strains.

3 NUMERICAL RESULTS

The application presented here aims to check the geomechanical coupling qualitative effect in two phase flow problem during reservoir production. Comparisons between the results of the flow simulations considering and not-considering the geomechanical coupling shows this effect.

The problem solved consists in two phase flow simulation of a ¼ five-spot three-dimensional reservoir considering three different situations: in the first one the reservoir is rigid (compaction phenomenon doesn't occur), in the second analysis the reservoir is elastic and the last analysis considers the reservoir as elastoplastic (Modified Cam-Clay).

The mechanical boundary conditions are null displacement in the symmetry boundary, while a stress state of 62 Mpa is applied in the opposite boundary (representing the side burden confinement), and in the top of reservoir (simulating the confinement imposed by overburden). The lower boundary is assumed to be fixed. The reservoir geometry consists in a volume of 140x130x60 meters and the finite element mesh used presents 1470 nodes and 1092 elements.

The reservoir has a initial pressure equal to 10 MPa and initial water saturation of 20%, the intrinsic permeability is $1x10^{-16}$ m², and porosity equal to 20%. The simulation time is equal to 1100 days with the producer well operating with a bottom hole pressure equal to 0.20 Mpa.

Figure 1 presents the accumulated oil and water production with time for the three analyses carried out. An increase in oil production is observed for the deformable reservoirs (elastic and plastic), showing the benefit achieved when the geomechanical effect is considered. When the plastic model is adopted the geomechanical effect in fluid production becomes more significant (increasing in oil production around 48%).

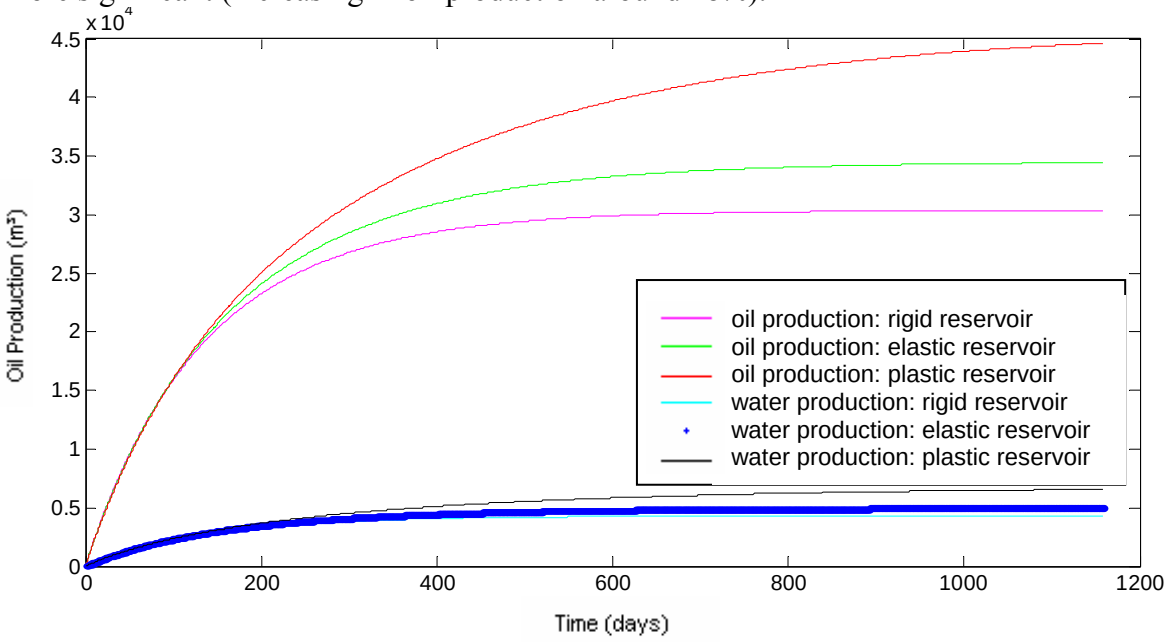

Figure 1. Accumulated oil and water production curve for rigid, elastic and plastic reservoirs.

Figure 2a shows the compaction curves for the plastic reservoir. The higher compaction occurs in the producer well zone, due to the high pressure decrease in this region. Figure 2b shows the distribution of preconsolidation pressure, indicating that all the reservoir yields.

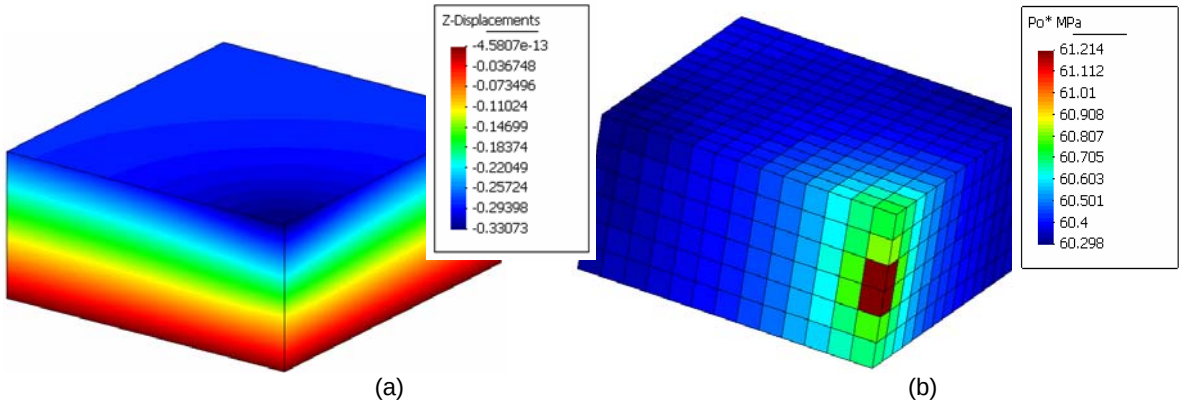

Figure 2. (a) Compaction distribution in the reservoir; (b)Distribution of overconsolidation stress .

4 CONCLUSIONS

The analyses presented in this paper show the consistency with the literature of geomechanical effects in hydrocarbon production in petroleum reservoirs due to decreasing in field pressure. This influence leads to porosity and permeability reduction that induce the fluid compression inside the reservoir, leading to oil production increase.

The plastic model defines more accurately the rock behavior and its stress distribution so oil production was higher than in the elastic case. Hence, the importance of the geomechanical coupling in petroleum reservoir studies is justified in this paper.

REFERENCES

[i] Onaisi, A.; Samier, P.; Koutsabeloulis, N.; Longuemare, P. 2002. Management of stress sensitive reservoirs using two coupled stress-reservoir simulation tools : ECL2VIS and ATH2VIS. Paper SPE 78512.

[ii] Wan, J. 2002. Stabilized finite element methods for coupled geomechanics and multiphase flow. Dissertation for the degree of Doctor of Philosophy. Stanford University.

[iii] Tran, D.; Nghiem, L.; Buchanan, L. 2005. An overview of iterative coupling between geomechanical deformation and reservoir flow. Paper SPE/PS-CIM/CHOA 97879 PS2005-396.

[vi] Gomes, I. F. 2006. Finite element implementation of the pressure na saturation equations to two phase flow simulation inside deformable petroleum reservoirs. PhD Thesys, Federal University of Pernambuco, Civil Engineering Departement, Recife, Brazil.

[v] Potts, D. M.; Zdravković, L. 1999. Finite element analysis in geotechnical engineering. Vol. 1, Published by Thomas Telford Publishing, London.

COUPLED HYDROMECHANICAL MODELLING OF RADIAL CO_2 INJECTION IN DEEP SALINE AQUIFERS

Víctor Vilarrasa[*], Diogo Bolster[†], Sebastià Olivella[†] and Jesus Carrera[*]

[*] GHS, Institute of Environmental Assessment & Water Research (IDAEA),
Consejo Superior de Investigaciones Científicas (CSIC)
Jordi Girona 18-26, 08034 Barcelona, Spain.
e-mail: victor.vilarrasa@upc.edu - Web page: http://www.h2ogeo.upc.es

[†] Department of Geotechnical Engineering and Geosciences
Technical University of Catalonia (UPC)
Campus Nord UPC, 08034 Barcelona, Spain

Key words: CO_2 sequestration, HM coupling, Two phase flow, Pressure buildup

Abstract. *Sequestration of carbon dioxide (CO_2) in deep saline aquifers has emerged as an option for reducing greenhouse gas emissions to the atmosphere. Due to the large amounts of CO_2 that will be injected into deep saline aquifers as a supercritical fluid, fluid pressure may increase dramatically around the injection zone. The simulations illustrate that, in a radial injection, fluid pressure rises sharply at the beginning of injection. However, once CO_2 fills the pores in the vicinity of the injection well, fluid flows more easily as CO_2 is about one order of magnitude less viscous than brine. As a result, fluid pressure drops, leading to a safer situation. The resulting overpressure may promote reactivation of sealed fractures or the creation of new ones in the caprock. This might lead to escape routes from the saline aquifer for the CO_2. To analyze the likelihood of such an event, we model an axysimetric horizontal aquifer-caprock system, including hydromechanical coupling. We study failure mechanisms and the conditions for these to occur considering a viscoplastic approach.*

1 INTRODUCTION

Carbon dioxide (CO_2) sequestration in deep saline aquifers is considered a promising mitigation option for the reduction of CO_2 emissions to the atmosphere. Injecting CO_2 into aquifers at depths greater than 800 m brings the CO_2 to a supercritical state where its density is large enough to ensure an efficient use of pore space[1]. However, CO_2 density will always be lighter than the resident brine. As such, it will flow along the top of the aquifer due to buoyancy. Thus, suitable aquifers should be capped by a low-permeability rock to avoid CO_2 migration to upper aquifers and the surface. Caprock discontinuities, such as fractured zones, may favor upwards CO_2 migration. Additionally, CO_2 injection can result in significant pressure buildup, which affects the stress field and may induce deformations. These can eventually damage the caprock and open new flow paths.

In practice, accounting for hydromechanical (HM) couplings permits us to determine

conditions at which mechanical failure (shear failure or hydraulic fracture) could occur, so that injection pressures can be limited below some fracturing threshold. Shear failure usually occurs at a lower injection pressure than hydro fracturing[2]. When the horizontal stress is greater than the vertical stress ($\sigma_h > \sigma_v$), shear failure will occur preferentially in shallowly dipping fractures, without damage to the upper part of the caprock. However, when the vertical stress is greater than the horizontal stress ($\sigma_h < \sigma_v$) the propagation of fractures is most likely to occur in the form of steeply dipping fractures which could go through the entire caprock[2].

Various injection schemes have been studied considering HM coupling, such as two-dimensional models that conceptually represent a large line of injection wells[3] and even a 3-D model simulating horizontal wells[4]. However, a single injection well with radial flow, which can be represented by an axysimetric model, has to the best of our knowledge not been studied yet.

2 PROBLEM SETUP

An ideal homogeneous horizontal aquifer-caprock system is considered for this study. The top of the 100 m thick aquifer is located at a depth of 1000 m. A 400 m thick low-permeability caprock overlies the aquifer and the caprock is covered by 600 m of media with low shear strength that do not need to be accounted for in the model. The system is axysimetric and extends laterally to 1 km. An injection well with a radius of 0.15 m is placed at the centre of the domain. The properties of the aquifer and caprock correspond to those of permeable sandstone and low-strength shale respectively. The initial conditions are hydrostatic pressure and constant temperature, which is taken as 320 K (the mean value for this aquifer). A constant head boundary condition is imposed in the outer boundary. CO_2 is injected uniformly throughout the entire thickness of the aquifer at a constant rate of 113 kg/s (3.6 Mt/yr). The initial conditions for the stress field are that the vertical stress is greater than the horizontal stress, $\sigma'_h = 0.65\sigma'_v$. The mechanical boundary conditions are no displacement normal to the bottom and outer boundary. The viscoplastic constitutive model adopted is explained somewhere else[5].

The injection of CO_2 into a homogeneous saline aquifer is simulated using the finite element numerical code CODE_BRIGHT[6,7]. To enable the simulation of CO_2 injection in a wide range of depths, CO_2 density[8] and viscosity[9] functions have been implemented at the code. Quadrilateral elements are used to enable the calculation of the mechanical problem. The mesh, which is unstructured, is made up with elements of size 10 m by 10 m close to the injection well, both in the aquifer and the caprock. The element size increases progressively with distance from the well attaining a maximum size of 30 m by 30 m at the outer boundary. As a first step, a steady-state calculation is carried out to obtain equilibrium initial conditions for the pressure and stress fields.

3 FLUID PRESSURE EVOLUTION

Figure 1 displays the evolution of fluid pressure at the top of the injection well. Injection

pressure increases sharply when CO_2 injection starts. This sharp increase is maintained until the region close to the well begins to desaturate and CO_2 starts flowing. As CO_2 fills the pores in the vicinity of the well, the fluid can flow more easily, because CO_2 viscosity is one order of magnitude smaller than that of brine. As a result, the injection pressure tends to drop or remain virtually constant. The magnitude of the pressure buildup is highly dependent on the permeability of the aquifer. Thus, the permeability of the aquifer may be a limiting factor.

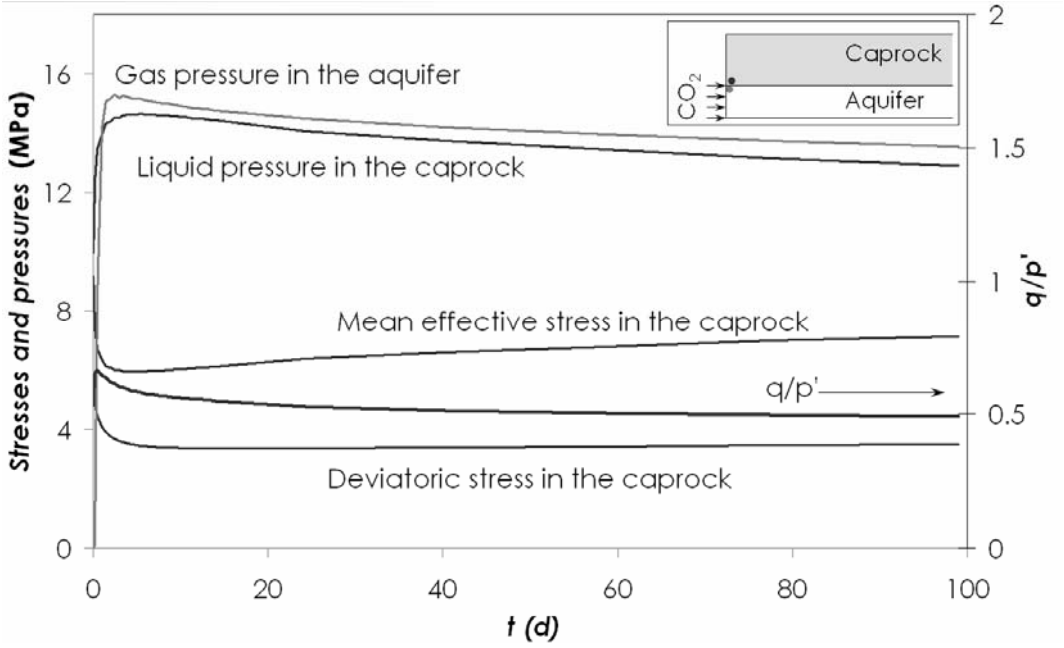

Figure 1. Stress and pressure evolution with time at the beginning of CO_2 injection at the base of the caprock next to the injection well (see location in inset).

4 HYDROMECHANICAL COULING

CO_2 injection causes fluid pressure to increase, thus changing the effective stress (Fig. 1). The latter produces deformations of the medium, which affect fluid pressure evolution. The mean effective stress is reduced much more than the deviatoric stress at the beginning of injection, which compromises the caprock integrity. This is the most critical moment, as indicated by the maximum in the ratio between the deviatoric and the mean effective stresses. After this, fluid pressure decreases, so the situation becomes safer from a mechanical point of view.

This is illustrated in Figure 2, where the (*q, p'*) plane for a point at the base of the caprock close to the well over an injection period of 100 days is represented. Prior to injection (point A), the caprock is in the safe zone, far from the plastification regime. Once injection begins, the mean effective stress decreases much more drastically than the deviatoric stress and the Mohr-Coulomb yield envelope is rapidly reached (point B). At this point, the rock reaches plastic behavior. Thus, strain occurs plastically for a few days, until it reaches point C after 5 days of injection. Then, the deviatoric stress decreases at a higher rate than over the period

between point B and C, and the caprock ceases to plastify. Finally, the mean effective stress increases, reaching a safe situation again (point D) after 100 days of injection. In this particular case the rock plastifies, but there will be injection scenarios in which the (*q, p'*) trajectory will not reach the Mohr-Coulomb envelope. In these situations, the mobilized angle of friction of the caprock, i.e. the angle of friction that sets the onset of plasticity, can be determined. This mobilized angle of friction yields an estimate for the likelihood of mechanical failure in a given situation. This leads to the definition of a safety factor (*SF*) that is defined as follows

$$SF = \frac{\tan \phi'_{real}}{\tan \phi'_{mobilized}}, \tag{1}$$

where in this particular case of injection, the mobilized angle of friction is 17.2º. Whenever the actual angle of friction of the caprock is higher than this mobilized angle of friction, the injection safety factor is higher than one, meaning that it will be safe.

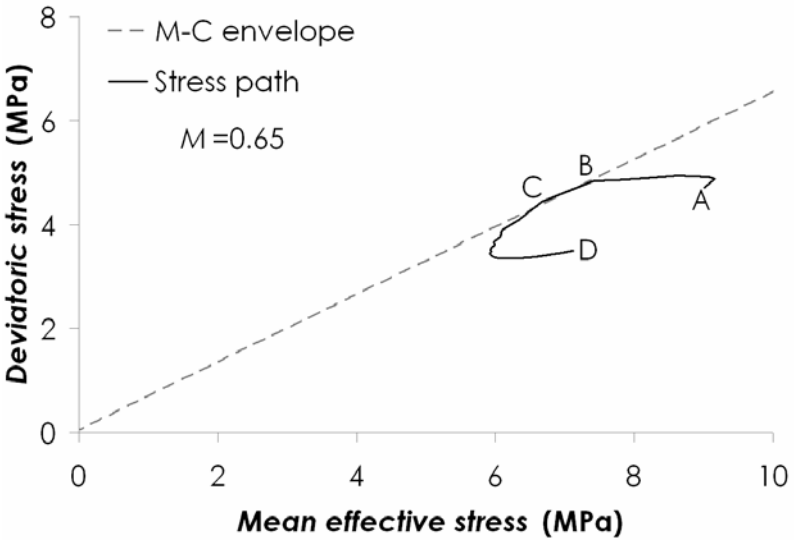

Figure 2. (*q, p'*) trajectory for a 100 day injection. The initial and final states are represented by A and D respectively. The onset of plasticity takes place during early times (B-C), but plastic behavior eventually stops. *M* has a low value to obtain irreversible strain.

5 CONCLUSIONS

- Fluid pressure drops when CO_2 fills the pores in the vicinity of the injection well because the viscosity of the CO_2 is one order of magnitude lower than that of the brine and consequently, fluid flows more easily.
- Slowly increasing the injection rate at the beginning is advisable so as to reduce the likelihood of damaging the caprock.
- Numerical simulations allow us to estimate the maximum sustainable injection pressure given the strength of the caprock. By means of determining the mobilized angle of friction, a safety factor can be defined.

REFERENCES

[1] Hitchon, B., Gunter, W. D., Gentzis, T. & Bailey, R. T., 1999. Sedimentary basins and greenhouse gases: a serendipitous association. *Energy Conversion & Management, 40,* 825–843.

[2] Rutqvist, J., Birkholzer, J. T. & Tsang, C-F., 2008. Coupled reservoir–geomechanical analysis of the potential for tensile and shear failure associated with CO_2 injection in multilayered reservoir–caprock systems. *Rock Mechanics and Mining Sciences, 45,* 132–143.

[3] Rutqvist, J. & Tsang, C-F., 2002. A study of caprock hydromechanical changes with CO_2 injection into a brine formation. *Environmental Geology, 42,* 296–305.

[4] Rutqvist, J., Vasco, D.W. & Myer, L., 2010. Coupled reservoir-geomechanical analysis of CO_2 injection and ground deformations at In Salah, Algeria. *International Journal of Greenhouse Gas Control, 4 (2),* 225–230.

[5] Vilarrasa, V., Bolster, D., Olivella, S. & Carrera, J., 2010. Coupled hydromechanical modeling of CO_2 sequestration in deep saline aquifers. *International Journal of Greenhouse Gas Control, submitted.*

[6] Olivella, S., J. Carrera, A. Gens, E. E. Alonso, 1994. Non-isothermal Multiphase Flow of Brine and Gas through Saline media. *Transport in Porous Media, 15,* 271–293.

[7] Olivella, S., A. Gens, J. Carrera, E. E. Alonso, 1996. Numerical Formulation for a Simulator (CODE_BRIGHT) for the Coupled Analysis of Saline Media, *Engineering Computations, 13 (7),* 87–112.

[8] Spycher, N., Pruess, K. & Ennis-King, J., 2003. CO_2-H_2O mixtures in the geological sequestration of CO_2. I. Assessment and calculation of mutual solubilities from 12 to 100ºC and up to 600 bar. *Geochimica et Cosmochimica Acta, 67 (16),* 3015–3031.

[9] Altunin, V. V. & Sakhbetdinov, M. A., 1972. Viscosity of liquid and gaseous carbon dioxide at temperatures 220-1300 K and pressure up to 1200 bar. *Teploenergetika, 8,* 85–89.